Journal of
Materials Chemistry C

Accepted Manuscript

This article can be cited before page numbers have been issued, to do this please use: J. Quinn, J. Zhu, X. Li, J. Wang and Y. Li, *J. Mater. Chem. C*, 2017, DOI: 10.1039/C7TC01680H.

ROYAL SOCIETY OF CHEMISTRY

rsc.li/materials-c

View Article Online
DOI: 10.1039/C7TC01680H

Journal Name

ARTICLE

Recent progress in developing n-type organic semiconductors for organic field effect transistors

Received 00th January 20xx,
Accepted 00th January 20xx

DOI: 10.1039/x0xx00000x

www.rsc.org/

Jesse T. E. Quinn,[a] Jiaxin Zhu,[a] Xu Li,[b] Jinliang Wang[b] and Yuning Li*[a]

This review highlights recent major progress in the development of organic semiconductors as electron transport n-channel materials in organic field transistors (OFETs). Three types of materials are discussed: 1) small molecules, 2) polymers, and 3) n-doped small molecules and polymers. Much efforts have been seen in the modification of known building blocks, development of novel building blocks, and optimizaiton of materials processing and device structures. These efforst have resulted in the achievement of record high electron mobilities for both small molecules (12.6 $cm^2V^{-1}s^{-1}$) and polymers (14.9 $cm^2V^{-1}s^{-1}$), which are approaching the highest hole mobilities achieved by p-type small molecules and polymers so far. In addition, n-doping of ambipolar and p-type organic semiconductors has proven to be an efficienct approach to obtaining a greater number of n-type organic semiconductors. However, it is found that n-type organic semicondcutors, in general, still lag behind p-type organic semiconductors in terms of carrier mobility and air stability. Further exploration of new building blocks for making novel materials and optimization of processing conditions and device structures are needed to improve the performance, particularly air stability.

1. Introduction

Organic field effect transistors (OFETs) or organic thin film transistors (OTFTs) employ organic semiconductors, either small molecules or polymers, as the channel layer, which can be more conveniently fabricated at much lower temperature, lower cost, and higher throughput in comparison to the conventional devices using inorganic semiconductors such as silicon.[1–3] In addition, organic semiconductors can be made soluble in solvents, enabling mass production of OFET-driven electronics by printing techniques. Organic semiconductors, particularly polymers, are much more mechanically robust and lighter than inorganic semiconductors. These appealing features offered by OFETs have opened up opportunities for the development of next generation electronic products such as flexible displays, ubiquitous radio-frequency identification (RFID) tags, wearable electronics, sensors, etc.[4–8] Charge carrier mobility of OFETs is the most important device parameter for many of the target applications of OFETs. Intrinsically organic semiconductors are inferior in terms of charge transport due to the nature of the weak secondary bonds (e.g., the van der Waals force) that hold the molecules together in comparison to inorganic semiconductors where ions and/or atoms are connected by the much stronger and shorter primary bonds such as ionic and covalent bonds.[1–3] The weaker intermolecular interaction results in the much larger intermolecular distances in organic semiconductors. Furthermore, the more complicated geometry of organic molecules compared with the simple, spherical atoms and ions that constitute the inorganic semiconductors render most of the organic semiconductors rather disordered. These factors make the charge transport within the organic semiconductors taking place dominantly in a hopping mode, which requires much higher energy compared with the band-like charge transport mechanism for inorganic semiconductors. Despite these structural disadvantages, over the past decades and especially in the past few years, remarkable improvements have been made in enhancing the charge carrier mobility of organic semiconductors, which are enabled by the development of new materials, improved materials processing, and device architecture optimization.[9–13,3,14,15] High mobilities of up to ~40 $cm^2V^{-1}s^{-1}$ for both single crystal[16,17] and aligned[18] small molecules and ~50 $cm^2V^{-1}s^{-1}$ for well-aligned polymers[19] have been achieved in OFETs. For solution processed (spin coated) OFET devices, high mobilities

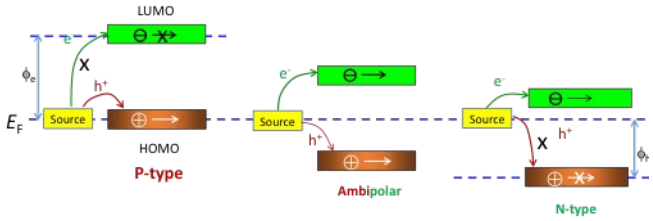

Figure 1. A schematic showing the relationships among the Fermi energy (E_F) of the source electrode, the frontier energies of the organic semiconductor, and the polarity of the majority charge carriers of the OFET device, where ϕe and ϕh denote the electron and hole injection barrier heights, respectively, and "X" denotes the inhibition of charge injection or transport.

[a] Department of Chemical Engineering and Waterloo Institute of Nanotechnology (WIN), University of Waterloo, 200 University Ave West, Waterloo, N2L 3G1, Canada.
[b] Institute of Chemistry, Henan Academy of Sciences, 56 Hongzhuan Road, Jinshui District, Zhengzhou, Henan, China, 450002.
*Corresponding author: a. E-mail: yuning.li@uwaterloo.ca; Fax: +1-519-888-4347; Tel: +1-519-888-4567 ext. 31105

View Article Online
DOI: 10.1039/C7TC01680H

Figure 2. Three types of commonly adopted OFET architecture (OSC: organic semiconductor): bottom-gate bottom-contact (BGBC), bottom-gate top-contact (BGTC), and top-gate bottom-contact (TGBC), where S, D, and G are the source, drain, and gate electrodes, respectively.

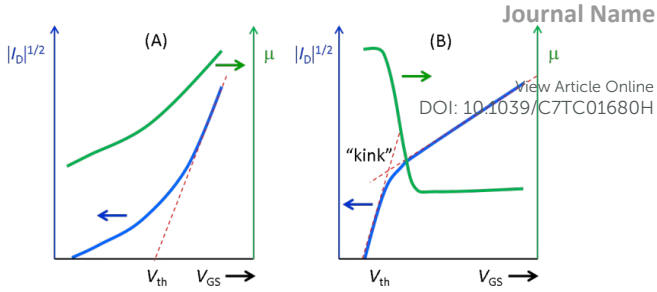

Figure 3. Two typical types of transfer curves in the saturation regime that severely deviate from the ideal MOSFET model, resulting in a dependence of mobility (μ) on the gate bias.

exceeding 10 $cm^2V^{-1}s^{-1}$ were reported for several polymer semiconductors.[20–23] These mobility values are far better than that of amorphous silicon (0.1-1 $cm^2V^{-1}s^{-1}$) and entered the mobility regime of multi-crystalline silicon. However, most of these high mobility values have been achieved for p-type organic semiconductors, which conduct holes in the OFET channel. For many electronic applications, n-channel OFETs using n-type organic semiconductors, which conduct electrons, are required to make complementary metal oxide (CMOS)-like logic circuits together with the p-channel OFETs. Unfortunately, much less n-type organic semiconductors have been reported and their mobility values are still lower compared with p-type organic semiconductors.[24–29]

One key reason for the lack of high performance n-type organic semiconductors is the much smaller number of available electron withdrawing building blocks that can be used for making n-type semiconductors with stable electron transport characteristics. When an electron is injected to the organic semiconductor in an OFET, it is equivalent to a reduction process in an electrochemical reaction. If the organic semiconductor has a rather high LUMO energy (or low electron affinity, EA), the injected electron residing in the LUMO of the semiconductor is at a high-energy state, which is prone to interact or react with some species such as the Si-OH groups on the SiO_2 dielectric surface and oxygen and H_2O in ambient air and thus the injected electrons are trapped or annihilated. Therefore, electron transport is weakened or inhibited (Figure 1). It has been theoretically proven and empirically demonstrated that a LUMO energy of ca. -4 eV or lower is required to realize a stable electron transport performance for an organic semiconductor.[30,29,31] A low LUMO energy would also reduce the electron injection barrier height (ϕ_e), which is the difference between the LUMO energy of the organic semiconductor and the Fermi energy (E_F) of the source electrode (Figure 1). Al, Ca and Ba, which have low work functions (or high Fermi energies), are favoured for electron injection; however, their thin films are prone to rapid oxidation and thus are difficult to handle. Instead, a more stable conductor, Au, is frequently used as the contacts for OFETs, although the work function (~5.1 eV, which is equivalent to a Fermi energy of -5.1 eV) of Au is not favoured for electron injection, but rather more favoured for the hole injection for p-channel OFETs. Therefore, large contact resistances are often observed for n-channel OFETs with Au contacts, which is another reason for the observed low electron motilities of many n-type organic semiconductors.

Most of the high mobility p-type and n-type polymer semiconductors reported so far have a D-A type structure, i.e., the repeat unit of these polymers is comprised of an electron donor (D) unit and electron acceptor (A) unit. Polymer main chains with such an alternating D-A arrangement would have a stronger intermolecular interaction, which shortens the π-π stacking distance and thus promotes the charge carrier hopping along the π-stacks. Some D-A polymers with strong electron accepting building blocks show very high electron mobilities; however, they also possess rather high HOMO energies due to the existence of the donor units, which creates insufficient hole injection barrier heights (ϕ_h) to block hole injections and allows stable hole transport in these semiconductors (Figure 1). As a result, these polymers exhibit ambipolar (electron and hole) charge transport characteristics, which are not desirable for CMOS-like logic circuit applications because ambipolar OFETs normally have high off current (I_{off}) and low current on-to-off ratio (I_{on}/I_{off}).[32] Furthermore, the OFET device architecture adopted also has an impact on the observed field transistor performance. Figure 2 shows the three types of OFET architecture often used, bottom-gate bottom-contact (BGBC), bottom-gate top-contact (BGTC), and top-gate bottom-contact (TGBC). TGBC n-channel OFETs exhibit better air stability and often higher electron mobility because the semiconductor layer is protected by dielectric and gate electrode layers from exposure to oxygen and moisture in ambient air. Lastly, the mobility values obtained by using the MOSFET (metal oxide semiconductor field effect transistor) model may be inaccurate since the mobility of organic semiconductors is often heavily dependent on the gate bias.[33–36] If the behaviour of an OFET obeys the MOSFET model, the field effect mobility (μ) in the saturation regime can be extracted using Equation (1):

$$I_D = \frac{\mu C_{diel} W}{2L}(V_{GS} - V_{th})^2 \qquad (1)$$

where I_D is the drain current, W and L are the channel width and length, C_{diel} is the capacitance per unit area of the dielectric, V_{GS} is the gate voltage, and V_{th} is the threshold voltage. The $|I_D|^{1/2}$ and V_{GS} would follow a linear relationship. However, many OFETs show a nonlinear $|I_D|^{1/2}$–V_{GS} plot with an increasing slope with the V_{GS} (Figure 3A), resulting in an increase of the mobility against the gate voltage with the mobility at the higher V_{GS} region significantly higher than at the lower V_{GS} region.[1,37,29,38] The cause for this nonlinearity has been accounted for by the existence of charge carrier traps residing at the disordered

DOI: 10.1039/C7TC01680H

molecular packing sites and structural defects in the semiconductor, in the dielectric layer close to the surface, and at the interface of the semiconductor and the dielectric, evidenced by the large $|V_{th}|$. Recently, several studies reported ultra-high mobility OFETs that showed a kinked $|I_D|^{1/2}$–V_{GS} curve (Figure 3B). These devices showed a much faster increase in the drain current (I_D) over a very small gate voltage range just above the threshold (V_{th}) compared to the high V_{GS} region, or so-called an "abrupt turn-on".[16,34–36] A recent study on the non-ideal behaviour of the single crystal rubrene OFETs revealed that the contact resistance (R_c) drops abruptly in the small V_{GS} region just above the V_{th}, which resulted in a higher mobility in the low V_{GS} region than in the high V_{GS} region extracted using the MOSFET model by more one order of magnitude. The mobility obtained from the low V_{GS} region was considered to be "overestimated" by some researchers.[35,36] The root cause for this "kinked" non-linear transfer curves is still not very clear. Takeya *et al*. explained this non-ideal behaviour observed for the single crystal rubrene OFETs by the charge carrier trapping and scattering at the semiconductor and dielectric interface.[16] Specifically, the mobility at a lower V_{GS} represents that of the in-crystal carriers, while the mobility at a higher V_{GS} become lower because more charge carriers were confined to the less ordered semiconductor/dielectric interface, where charge carrier trapping and scattering occur. Recently, Pei *et al*.[23] found that the non-ideal characteristic of a high mobility n-type polymer is correlated to the microstructures of the polymer films, i.e., higher crystallinity films having larger crystallite domains and better stacking order led to more frequent occurrence of non-ideal kinked transfer curves. Nonetheless, overly inaccurate mobility values, which are either overestimated or underestimated from the non-ideal OFET behavior, may provide erroneous structure-property relationships of organic semiconductors and mislead the chemists when designing organic semiconductors.[36] Therefore, cautions should be applied when correlating the reported carrier mobilities with the chemical and nano-/microscale structures of the materials. In addition to a high charge carrier mobility, a high I_{on}/I_{off} ratio, a small V_{th}, and a small subthreshold swing are other desirable OFET parameters, which are critically required for many applications of OFETs.[24]

This article provides a review on the major advancement in the development of new n-type organic semiconductors, including small molecules and polymers, with high electron mobilities of about 0.1 $cm^2V^{-1}s^{-1}$ (the lower limit for amorphous silicon) or higher, in the past five years. Some relevant materials reported earlier are also included for the convenience of discussion. Through this review, we aim to provide new insight into the relationship between the structure (types of acceptor building blocks, crystallinity, morphology, etc.) and property (the LUMO and HOMO energies, air stability, as well charge carrier mobilities, etc.) of n-type organic semiconductors. We hope the newly acquired knowledge and findings summarized in this review will benefit the chemists and materials scientists in this field for the development of better organic semiconductors for OFETs and other applications.

2. Small molecule n-type organic semiconductors

2.1. Rylene diimide-based derivatives

Naphthalene tetracarboxylic diimides (NDIs) are among the first small molecule n-type organic semiconductors that demonstrated great potential for OFETs (Figure 4, and Table 1).[39–41] For example, the single crystal *N*-cyclohexyl substituted NDI, **S1**, exhibited high electron mobility of 7.5 $cm^2V^{-1}s^{-1}$.[42] However, the OFET devices with *N*-alkyl substituted NDIs degrade readily under ambient conditions due to their inadequately low LUMO energies to prevent the detrimental reactions with moisture and oxygen. Introduction of fluorinated side chains was found to be able to achieve a denser molecular packing to prevent the diffusion of oxygen and moisture[43] as well as to lower the LUMO energy from -3.64 eV for the alkylated NDI to -3.71 ~ -3.82 eV for the semifluoroalkylated NDIs.[44] Improved air stability of the OFETs with these semifluoroalkyled NDIs was observed. *N*-*p*-(trifluoromethoxy) benzyl ($BOCF_3$) substituted NDI, **S2** (**NDI-BOCF$_3$**), also showed improved air stability in OFETs, but the electron mobilities reported previously were quite low (~10^{-2} $cm^2V^{-1}s^{-1}$).[45,46] Recently, Zhang *et al.* revisited this compound and found that **S2** has a surprisingly low LUMO energy of -4.20 eV, which was accounted for by the strong electron accepting effect of the $BOCF_3$ side chains. OFETs with this compound showed an electron mobility of 0.7 cm^2V^{-1} s^{-1} with an I_{on}/I_{off} of 10^6 in ambient air.[47] Recent endeavors have been made to obtain air-stable NDIs by incorporating electron-withdrawing groups such as cyano and halogen groups to the naphthalene core in order to lower their LUMO energy levels.[39,47,48] Lee *et al.* demonstrated that chlorination of the NDI core with two or four electron-withdrawing chlorine atoms could enhance air stability of the resulting materials.[49] The dichloro and tetrachloro NDIs showed LUMO energies of -4.01 eV and -4.13 eV, respectively, which are much lower than that of the non-chlorinated NDI compound (-3.72 eV). The dichlorinated **S3a** (**Cl$_2$-NDI**) with *N*-fluoroalkyl substitution showed the highest electron mobility of 0.57 $cm^2V^{-1}s^{-1}$ for OEFTs processed by solution-shearing deposition and 0.86 $cm^2V^{-1}s^{-1}$ for OFETs processed by vacuum deposition. He *et al.* achieved electron mobilities as high as 8.6 $cm^2V^{-1}s^{-1}$ with I_{on}/I_{off} of ~10^7 for the single crystal **S3a** in ambient conditions.[50] The molecules were packed in a face-to-edge herringbone structure with a very short π-π stacking distance of 0.327 nm. It was found that the C-H···O interactions existed, which might facilitate electron tunneling between the π-stacks. The mobility only decreased by 13% after the device was kept in ambient air for 82 days (Figure 5). Yuan *et al.* recently performed a systematic study on the core-fluorinated NDIs.[48] The di- or tetra-fluorinated NDIs have slightly lower LUMO energies, which are in a range between -3.73 eV and -3.97 eV depending on the side chains and the number of F, than that of the non-substituted (-3.63 eV). However, they exhibited lower mobilities than their core-chlorinated NDI counterparts. The best mobility of 0.1 $cm^2V^{-1}s^{-1}$ was obtained for the difluoro core-substituted NDI **S3b**.

View Article Online
DOI: 10.1039/C7TC01680H

Compound	Acronym	E_{LUMO}/E_{HOMO}, ev	Device structure-source-drain material/deposition method (SX: single crystal; VD: vacuum deposition; SP: spin coating; SD: drop coating	μ_e or μ_e/μ_h, $cm^2V^{-1}s^{-1}$	I_{on}/I_{off}	V_{th}, V	Test atm.	Retention of μ_e/ storage time in ambient air	Year [Ref.]
S1			BGTC-Au/VD	7.5	10^8	58	Ar		2008 [42]
S2	**NDI-BOCF$_3$**	-4.22/-7.20	BGTC-Au/VD	0.7	10^6	21	air		2016 [47]
S3a	**Cl$_2$-NDI**	–4.01/-	BGTC-Au/ shear BGTC-Au/VD BGTC-Au/SX	0.57 0.86 8.6	10^6 10^7	-11 9	N_2 N_2 air	87%/82 d	2011 [49] 2011 [49] 2013 [50]
S4	**NDITz**	-3.99/-6.37	BGBC-Au/SP	0.15	10^7	13-18	air		2013 [51]
S5a	**NDI2ODDTYM2**	-4.3/-	BGTC-Ag/SP	0.51	10^6-10^7	2-9	air		2010 [52]
S5b	**NDI3HU-DTYM2**		BGBC-Au/SP	3.50	10^8	0.17	air		2013 [53]
S5c			BGTC-Au/SP	0.70	10^7	7	air		2012 [54]
S6		–3.94/-	BGTC-Au/SP	0.45	10^5-10^6	21-36	air		2017 [55]
S7a	**C8-NDTI**	-4.0/-6.1	BGTC-Au/VD	0.05	10^8	10	air		2013 [56]
S7b		-4.1/-	BGTC-Au/VD	0.73	10^5	1.9	air		2015 [57]
S8	**F-NDTI**	-4.16/-6.31	BGTC-Au/SX	1.59	10^4	-2	air		2016 [58]
S9	**NDINI**	-4.20 /-6.68	BGTC-Au/SX	1.75 1.55	10^6		N_2 air		2016 [59]
S10	**C12-4CldiPBI**	-4.22/-6.04	BGTC-Ag/SX	4.65	10^5		air	100%/50d	2012 [60]
S11b	**NDI-*cis*-S2**	-4.11/-6.46	BGBC-Au/SP	0.075	10^6	19	N_2		2015 [61]
S12d	**PDI-S4**	–4.12/	BGBC-Au/SP	0.19	10^3	12	N_2		2015 [62]
S13	**BTI5**	-3.55/-5.48	TGBC/SP	0.045/10^{-3}			N_2		2017 [63]
S14a	**CF$_3$-TPDO**	-3.67/-6.04	BGTC-Au/VD	0.07	10^6	60	air	94%/30d	2008 [64]
S15d	**TIPS-TPDO-4CN**	-4.18/-6.71	BGTC-Ag/VD	0.11	10^6		air	80%/30d	2015 [65]
S16	**OANQ**	-4.32/-6.01	BGTC-Ag/VD	0.2	10^5		air	100%/30d	2015 [66]
S17a	**DAzBT**	-/-5.43	BGTC-Au/VD	0.024	10^6	-25	N_2		2012 [67]
S17b	**DAzTT**	-/-5.45	BGTC-Au/VD	0.05	10^5	-5	N_2		2012 [67]
S18a	**TAz1**	–3.93/-5.56	BGTC-Au/VD	0.29	10^7	37.1	N_2		2013 [68]
S18c	**TAz3**	-3.90 /-5.47	BGTC-Al/VD	0.31			N_2		2016 [69]
S18d	**TAZ4**	-3.93 /-5.59	BGTC-Au or Al/VD	0.15			N_2		2016 [69]
S19	**BAzDI-2**	-3.74/-5.43	BGTC-Au/SP	0.015	10^4-10^5	50-65	N_2		2016 [70]
S20		-3.99/-5.91	BGTC-Au/SP	0.16	10^5-10^6	27-38	N_2		2017 [71]
S21		-4.3/	BGTC-Au/SP	0.9	10^5		air	~50%/87d	2011 [72]
S22a	**2DQTT-*o***	-4.51/-5.62	BGBC-Au/SP	3.0	10^6	–1.4	air		2014 [73]
S22b	**2DQTT-*o-B***	–4.44/ –5.59	BGBC-Au/SP	5.2	10^6	–13.9	air		2016 [74]
S22c	**2DQTT-o-*L***	–4.44/ –5.59	BGBC-Au/SP	0.36	10^2	–10.9	air		2016 [74]
S23a	**2DQTT-*i***	-4.77/-5.93	BGBC-Au/SP	0.44	10^3	2.6	air		2014 [73]
S23b	**2DQTT-*i-B***	–4.54/–5.57	BGBC-Au/SP	0.1	10^4	5.2	air		2016 [74]
S23c	**2DQTT-*i-L***	–4.54/–5.57	BGBC-Au/SP	0.48	10^4	0.8	air		2016 [74]
S24	**TFT-CN**	-4.15/-5.72	BGTC-Au/SP BGTC-Au/ribbon	1.11 7.7	10^5 10^4	7.1 -10	N_2		2016 [75]
S25a	**C20-DBTII**	-3.72/	TGBC-Au/SP	0.011/5.72 × 10^{-4}	10^2/10^2	47/-53	air		2015 [76]
S25b	**C20-DBFII**	-3.73/-5.52	TGBC-Au/SP	0.074	10^4	40	air		2015 [76]
S26a	**BDOPV**	-3.64/-5.98	BGTC-Au/SX	3.25	10^6	7.91	air (RH=50-60%)	>75%/30d	2015 [77]
S26b	***o*-F$_2$-BDOPV**	-3.84/-6.18	BGTC-Au/SX	2.60	10^3	0.52	air (RH=50-60%)	>75%/30d	2015 [77]
S26c	***p*-F$_2$-BODPV**	-3.84/-6.13	BGTC-Au/SX	6.55	10^3	11.54	air (RH=50-60%)	>75%/30d	2015 [77]
S26d	**F$_4$-BDOPV**	-4.03/-6.32	BGTC-Au/SX	12.6	10^6	8.71	air (RH=50-60%)	~80%/30d	2015 [78]
S26e	**F$_6$-BDOPV**	-4.10 /-6.40	BGTC-Au/SX	4.66	10^3	–8.38	air (RH=50-60%)	>75%/30d	2015 [77]
S27a	**QBT**	-3.76/-5.25	TGBC-Au/ SP	5.0 × 10^{-3}/3.1 × 10^{-2}	10^{5-6}/10^{7-8}	49.4/–39.1	N_2		2015 [79]
S27b	**QBS**	-3.73/-5.33	TGBC-Au/SP	2.1 × 10^{-2}/5.5 × 10^{-2}	10^{4-5}/10^{6-7}	35.9/–41.1	N_2		2015 [79]
S28a	**IDTO**	-3.99 /-5.85	BGBC-Au/SP	0.046	10^5	5.3-7.9	N_2		2016 [80]
S25b	**IDTO-5Br**	-4.12 /-6.33	BGBC-Au/SP	0.071	10^5	12-15	N_2		2016 [80]
S25c	**IDTO-6Br**	–4.18 /-6.30	BGBC-Au/SP	0.11	10^5	2.1-4.9	N_2		2016 [80]

Table 1 Summary of properties of n-type small molecule semiconductors.

View Article Online
DOI: 10.1039/C7TC01680H

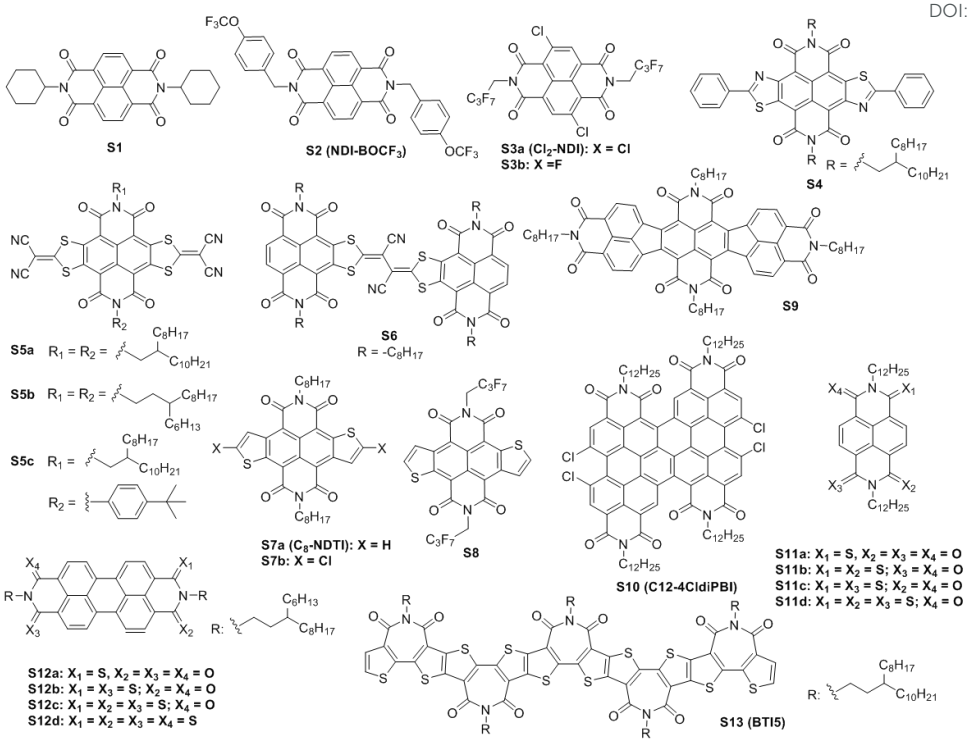

Figure 4. Naphthalene tetracarboxylic diimide (NDI) and perylene diimide (PDI).

Fusion of π-conjugated moieties to the NDI core (core-expansion) is another effective approach to lowering the LUMO energy of NDIs.[81,54,52] The dithiazole-fused NDI, **S4** (**NDITz**),[51] has a LUMO energy of -3.99 eV, about 0.1 eV lower than that of the non-core fused NDIs. Electron mobilities of up to 0.15 $cm^2V^{-1}s^{-1}$ and high I_{on}/I_{off} of ~10^7 were obtained under ambient conditions. Gao *et al.* fused two 2-(1,3-dithiol-2-ylidene)malonitrile groups to the NDI core by a simple nucleophilic aromatic substitution reaction.[52] The resulting core-expanded NDI (**S5a**) exhibited a LUMO energy of -4.3 eV, which is much lower than that of the unsubstituted NDI and warrants the air stability of **S5a** in n-channel OTFTs. Under ambient conditions electron mobilities as high as 0.51 $cm^2V^{-1}s^{-1}$ with I_{on}/I_{off} of 10^5-10^7 were achieved for the spin coated **S5a** thin films (annealed at 180 °C) in BGTC devices with Ag contacts. By moving the branching point of the sidechains one CH_2 farther from the NDI core, the mobility of the resulting **S5b** was greatly improved to 3.50 $cm^2V^{-1}s^{-1}$ in the BGBC device architecture with Au contacts.[53] The position of branching point was found to cause critical changes in molecular packing and thus the electron mobility. The high mobility of **S5b** was attributed to its dense in-plane molecular packing and large crystal domains (~1 μm × 3 μm). The devices showed comparable performance in ambient air and nitrogen, indicating the good air stability of this compound. The same group developed a mild and versatile one-pot synthetic route to a variety of core-expanded naphthalene diimides with symmetric and unsymmetrical substituents.[54] One unsymmetrically substituted product, **S5c**, achieved good electron mobility of 0.70 $cm^2V^{-1}s^{-1}$ with an I_{on}/I_{off} of 10^7 under ambient conditions. More recently, an NDI-based dimer bridged by a (1,3-dithiol-2-ylidene)acetonitrile moiety (**S6**) was synthesized. The as-spun **S6** thin films showed electron mobilities as high as 0.45 $cm^2V^{-1}s^{-1}$ with high I_{on}/I_{off} of up to ~10^6.[55] Fukutomi *et al.* incorporated two thiophenes to the NDI core forming naphthodithiophenediimides (NDTIs).[56] The *N*-octyl substituted NDITI, **S7a** (**C_8-NDTI**), has a lower LUMO energy of -4.0 eV than that of its NDI counterpart (-3.9 eV) due to the more extended π-conjugation enabled by the additional two thiophene moieties. Vacuum deposited **S7a** films exhibited electron mobilities as high as 0.05 $cm^2V^{-1}s^{-1}$ with an I_{on}/I_{off} of 10^5 under ambient conditions. By adding chloro substituents at the α-positions of the thiophene moieties, the new derivative **S7b** has a further lower LUMO energy of -4.1 eV.[57] The two chloro atoms enabled the Cl···O–C contacts, which played a role to form a two-dimensional (2D) bricklayer structure. In contrast, **S7a** without chloro substitution formed a herringbone-like one-dimensional (1D) electronic structure. The 2D-like electronic structure of **S7b** helped charge transport, achieving a much higher electron mobility of 0.73 $cm^2V^{-1}s^{-1}$ for the vacuum deposited films. Fan *et al.* reported an *N*-fluoroalkyl NDTI, **S8**, which has very low LUMO and HOMO energies of -4.16 eV and -6.31 eV, respectively.[58] The molecular packing of a single crystal **S8** belongs to the $P2_1/c$ space group with a short π–π distance of 3.40 Å. OFETs with single crystal **S8** achieved high electron mobilities of up to 1.59 $cm^2V^{-1}s^{-1}$ with an I_{on}/I_{off} of 10^4 in BGTC devices in ambient air. Lately, Wang *et al.* fused two naphthalene imide units to NDI, forming **S9** (**NDINI**), which has very low LUMO and HOMO energies of -4.20 eV and -6.68 eV, respectively.[59] Spin coated **S9** films showed rather low electron

View Article Online
DOI: 10.1039/C7TC01680H

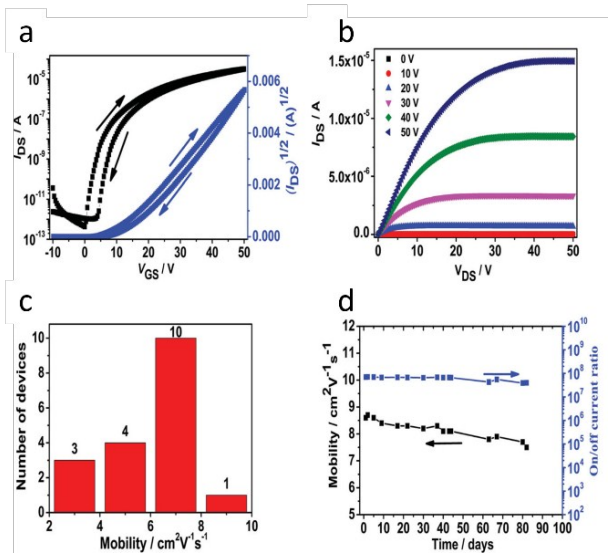

Figure 5. (a) and (b) Transfer and output curves of an OFET with a ribbon-shaped **S3a**. (c) The mobility distribution of 18 devices. (d) Stability of devices over time in ambient air at room temperature. Reproduced with permission from ref. 50. Copyright 2013 John Wiley & Sons.

mobility of 7.4 × 10^{-4} $cm^2V^{-1}s^{-1}$ due to the poor film quality (poor morphology). However, the single-crystalline microfibers exhibited electron mobility as high as 1.75 $cm^2V^{-1}s^{-1}$ with an I_{on}/I_{off} of 10^6 in OFETs measured in nitrogen. When measured in air, the mobility was only slight lower (up to 1.55 $cm^2V^{-1}s^{-1}$).

Similar to NDIs, perylene diimides (PDIs) are also a class of initially well-studied n-type semiconductor materials.[40,41] They have particularly received increasing interest as very promising non-fullerene acceptors for low-cost OPVs.[82,83] For the OFET application, a noteworthy perylene derivative, diperylene bisimide **S10** (**C12-4CldiPBI**), was reported by Wang *et al.*[60] **S10** has deep LUMO and HOMO energies of -4.22 eV and -6.04 eV, respectively. An "Au stripe mask" technique was used to fabricate OFETs with small single crystal ribbons of **S10**. Very high electron mobilities of up to 4.65 $cm^2V^{-1}s^{-1}$ were achieved under ambient conditions. The devices showed no obvious degradation after being kept in air for 50 days.

Substitution of the imide oxygen for sulfur (thionation) is recently reported to be a simple and efficient way to lower the LUMO energy and promote the electron transport of NDI[61,84] and PDI[62] derivatives. Kozycz *et al*. found that as the degree of thionation increases the LUMO energy decreases gradually from -3.79 eV for the non-thionated NDI to -4.30 eV for the terthionated NDI, **S11d**.[61] On the other hand, the HOMO energies of the thionated NDIs became higher at ca. -6.4~-6.5 eV than that (-6.97 eV) of the non-thionated NDI, leading to smaller band gaps of the thionated NDIs. These band energy changes are considered due to the involvement of the large sulphur atoms in the core conjugation. All the thionated NDIs showed dramatic increases in electron mobilities to ~10^{-2} $cm^2V^{-1}s^{-1}$ (the best mobility of 7.5 × 10^{-2} $cm^2V^{-1}s^{-1}$ was achieved for **S11b**) with respect to the electron mobilities of ~10^{-5} $cm^2V^{-1}s^{-1}$ for the non-thionated NDI compound. Similar trends were observed for the thionated PDI compounds **S12**'s.[62] The LUMO energy decreases with the degree of thionation from -3.67 eV for the parent PDI compound to -4.12 eV for the tetrathionated PDI **S12d**. Among this thionated PDIs, **S12d** showed the best n-type semiconductor performance with the highest mobility of 0.19 $cm^2V^{-1}s^{-1}$ in OFETs owing to the combined effects of its lowest LUMO energy, favoured crystal structure, as well as the improved grain boundaries.

A bithiophene linked by an alkylimide group at the ,3,3'-postions, *N*-alkyl-2,2'-bithiophene-3,3'-dicarboximide unit (BTI), was used by Marks *et al.*[85] as an electron deficient building block to make air-stable n-type, ambipolar, and p-type polymers in OFETs with mobilities in the order of 10^{-2} $cm^2V^{-1}s^{-1}$. Guo *et al.* very recently reported a series of well-defined oligomers with 2 to 5 fused BTI units.[63] These ladder-type BTI derivatives showed promising electron-transporting characteristics with electron mobilities of 10^{-2} $cm^2V^{-1}s^{-1}$ in TGBC OFETs. The largest molecule in this series, **S13** (**BTI5**), has a LUMO energy of -3.55 eV and exhibited the highest electron mobility of 0.045 $cm^2V^{-1}s^{-1}$. Higher mobility may be achieved if the bulky 2-octyldodecyl side chains are replaced with smaller side chains to improve the molecular packing.

2.2. *N*-Heteroacenes

N-Heteroacenes, where some of the carbon atoms of acenes are replaced by nitrogen atoms that render these compounds more electron deficient, represent a class of promising n-type semiconductors for OFETs.[86] Among them, the triphenodioxazine (TPDO) structure has been of particular interest because this five-ringed structure resembles pentacene that is one of the mostly studied small molecule p-type semiconductors. Early in 2008 Di *et al.* reported a trifluoromethyl-substituted TPDO **S14a** (**CF_3-TPDO**).[64] The electron withdrawing TPDO core and CF_3 substituents at the para-positions to the nitrogen atoms helped lowering the LUMO energy to -3.67 eV. OFET devices with vacuum deposited **S14a** films showed good air stability and electron mobility of ~0.07 $cm^2V^{-1}s^{-1}$ with a high I_{on}/I_{off} of 10^6. **S14b** with CF_3 substituents at the para-positions to the oxygen atoms has an identical LUMO energy as that of **S14a**, but showed lower mobilities around 0.01 $cm^2V^{-1}s^{-1}$. Both **S14a** and **S14b** showed good air stability with minimal changes in electron mobility after 30 days. The LUMO energy (-3.67 eV) of these compounds seems insufficient for achieving air stable electron transport. It was suggested that the close crystal packing enabled by the introduction of CF_3 substituents could prevent the diffusion of oxygen, which accounted for the good air stability of these compounds. Triisopropylsilyl (TIPS) has been used for the substitution of pentacene to improve the solubility and obtain favourable solid state packing of the resulting TIPS-pentacene (Figure 6), which is a high performing p-type semiconductor.[87] Nicolas *et al*. reported TIPS-TPDO,[88] **S15a**, which is a direct analogue of TIPS-pentacene. **S15a** showed n-type semiconductor performance. However, the electron mobilities of the **S15a** based OFETs are quite low in the order of ~10^{-3} $cm^2V^{-1}s^{-1}$. The same research group later synthesized a series of TIPS-TPDOs with two or four CN substituents on the TPDO core.[65] The products **S15b** and **S15c**, which have two CN substituents, have LUMO energies of -3.79 eV and -3.81 eV, respectively, measured by cyclic

View Article Online
DOI: 10.1039/C7TC01680H

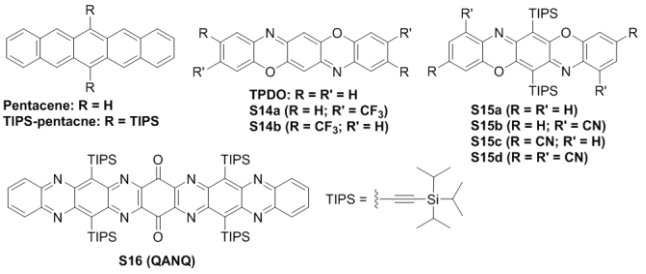

Figure 6. Pentacenes and *N*-heteroacenes.

voltammetry (CV). **S15d** (**TIPS-TPDO-4CN**) with four CN substituents has the lowest LUMO energy of -4.18 eV. Among these series, **S15d** achieved the best performance with the average electron mobilities of 0.014 and 0.10 $cm^2V^{-1}s^{-1}$ (with a maximum of 0.11 $cm^2V^{-1}s^{-1}$) for the spin coated and vacuum evaporated films in OFETs using Ag contacts in ambient conditions. The devices retained 80% of the initial mobility after 30 days storage in air, demonstrating the excellent air stability of this material. More recently, the same group used **S15d** as the semiconductor and the cross-linked poly(methyl methacrylate) (*c*-PMMA) as dielectric to fabricate OFETs on polyethylene terephthalate substrate.[89] The devices demonstrated a maximum electron mobility of 1.8×10^{-2} $cm^2V^{-1}s^{-1}$ and an I_{on}/I_{off} of 10^5, which are promising for flexible applications.

Wang *et al.* reported a large 9-ring *N*-heteroacene, **S16** (**OANQ**).[66] The single-crystal structure of **S16** reveals a slightly twisted motif, which may play a role in enhancing the stability by reducing the strain generated from the π interactions and steric effects of the side chains. The 2D "brick layer" face-to-face stacking structure and the strong π-π interactions are considered favourable for large transfer integrals and 2D electron transport. A very low LUMO energy of -4.32 eV was measured. Single crystals of **S16** were tested in OFETs with Ag source and drain contacts. The highest electron mobility of 0.2 $cm^2V^{-1}s^{-1}$ with an I_{on}/I_{off} of up to 10^5 was obtained under ambient air. Devices showed no obvious degradation in performance after storage for one month under ambient conditions, demonstrating excellent air stability of this material.

2.3. Azulene derivatives

Azulene, a resonance-stabilized aromatic isomer of naphthalene, consists of a seven-membered ring and a five-membered ring, which displays a large dipole moment of 1.08 D (Figure 7).[69,90] Application of azulene in constructing organic optoelectronic materials was recently reviewed by Gao [91] and Zhang *et al.*[92] In 2012 Yamaguchi *et al.* first reported the synthesis, properties, and OFET characteristics of two azulene-based derivatives 5,5'-di(2-azulenyl)-2,2'-bithiophene **S17a** (**DAzBT**) and 2,5-di(2-azulenyl)-thieno[3,2-*b*]thiophene **S17b** (**DAzTT**).[67] These compounds showed p-type semiconductor performance with hole mobilities of 10^{-2} $cm^2V^{-1}s^{-1}$ and I_{on}/I_{off} of 10^5–10^6 in OFETs. No reduction peaks were observed in the CV diagrams of these compounds and therefore the LUMO energies were not reported in this paper. However, based on

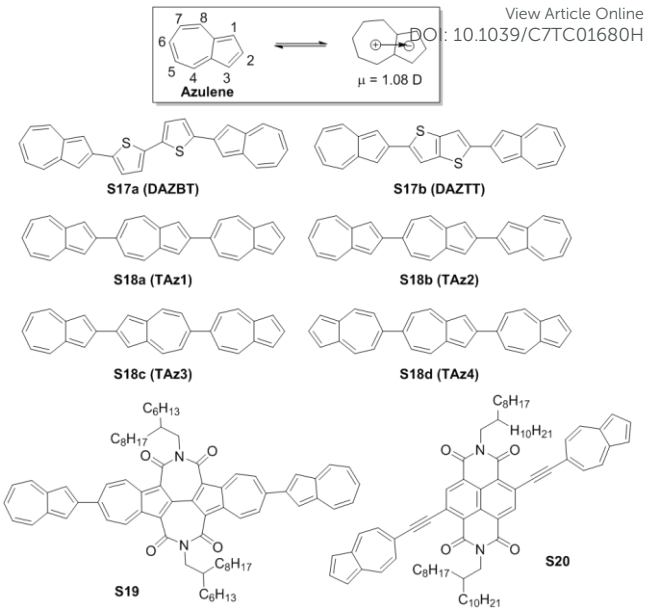

Figure 7. Azulene and its derivatives.

the reported HOMO energies and optical band gaps, the LUMO energies of **S17a** and **S17b** can be estimated to be -3.69 eV and -3.71 eV, respectively. An extension of this work was reported by the same group in the following year.[68] Three azulene units were connected linearly in the same direction to form 2,6':2',6''-terazulene **S18a** (**TAz1**). **S18a** has a narrow E_g^{opt} of 1.63 eV with a HOMO energy of -5.56 eV and a low LUMO level at −3.93 eV. Bottom-gate top-contact (Au or Al) OFETs with 60 nm-thick vacuum deposited **S18a** thin films on octadecyltrichlorosilane (ODTS)-treated Si/SiO_2 substrate at different substrate temperatures (room temperature, 60 °C, and 100 °C) were fabricated. All devices showed unipolar n-channel performance. A maximum electron mobility of 0.29 $cm^2V^{-1}s^{-1}$ and an I_{on}/I_{off} of 10^7 were achieved at a substrate temperature of 100 °C. It is interesting to note that **S18a** as a hydrocarbon molecule showed electron transport, not hole transport, performance. The authors conducted DFT calculations on this molecule and found that the LUMO is quite evenly distributed, while the HOMO is localized at one end of the molecule. Therefore, for two molecules packed with an antiparallel orientation, the LUMOs can overlap, but HOMOs cannot. This explains the observed electron-only charge transport performance of this molecule. The single crystal XRD data confirmed the coexistence of both parallel and antiparallel orientations at a 1:1 ratio. Very recently, Yamaguchi *et al.* thoroughly studied a series of terazulenes, **S18b**, **S18c**, and **S18d**, which are regioisomers of **S18a**.[69] The LUMO/HOMO energies decrease in the order of **S18b**, **S18c**, and **S18d** with values of -3.83 eV/-5.45 eV, -3.90 eV/-5.47 eV, and -3.93 eV/-5.59 eV, respectively. **S18b** showed unipolar p-type transistor performance for all devices with Au contacts, achieving a highest hole mobility of 1.32 $cm^2V^{-1}s^{-1}$. When the low work function Al contacts were used, hole transport only performance was observed for the devices fabricated on substrates heated below 60 °C, while ambipolar charge transport was observed for devices fabricated at a

View Article Online
DOI: 10.1039/C7TC01680H

substrate temperature of 100 °C. **S18c** showed unipolar electron charge transport at most annealing temperatures with either Au or Al contacts except for the ones with films deposited at room temperature and Au as contacts, which showed ambipolar performance. The highest electron mobility of 0.31 $cm^2V^{-1}s^{-1}$ for **S18c** was obtained for the device with the film deposited at 100 °C and Al as contacts. **S18d** showed unipolar n-type semiconductor performance in all devices with electron mobility of up to 0.15 $cm^2V^{-1}s^{-1}$. Based on the device data, it seems that the 2,2-biazulene unit (as in **S18b** and **S18c**) accounted for the p-type characteristics. This was explained through the molecular orbital distribution supported by the B3LYP/6-31G calculations. **S19** (**BAzDI-2**), an azulene-based aromatic diimide, which comprises of a 2,2'-biazulene moiety and two seven-membered imide groups, has a LUMO energy level of -3.74 eV and showed a moderate electron mobility of 1.5×10^{-2} $cm^2V^{-1}s^{-1}$ and I_{on}/I_{off} of 10^4–10^5 in BGTC devices using Au contacts in nitrogen.[70] Judging the relatively high LUMO energy of this compound, the devices are probably not stable in air, although it was not mentioned in the paper. Recently, Gao *et al.* reported an ethynylazulene end-capped NDI **S20**,[71] which showed a LUMO energy of -3.99 eV that is similar to that of the unsubstituted NDIs. The highest electron mobility of 0.16 $cm^2V^{-1}s^{-1}$ and I_{on}/I_{off} of 10^5–10^6 were achieved under nitrogen conditions in BGTC devices.

2.4. Quinoidal oligothiophenes

Dicyanomethylene-terminated quinoidal oligothiophenes (QOTs) are a class of well-studied n-type semiconductors.[93–95] However, the electron mobilities of QOTs have been much lower than 1 $cm^2V^{-1}s^{-1}$, a bottleneck that has been attributed to the smaller π-surface of QOTs, which negatively affects the transfer integral magnitude that relates to the charge transport in organic semiconductors.[73] In 2011, Zhu *et al.*[72] synthesized a solution processable dicyanomethylene-substituted fused tetrathienoquinoid, **S21** (Figure 8), which enhances the intermolecular interactions and eliminates the problem of *cis*/*trans*-isomerism that can occur in their QOT counterparts. **S21** has a deep LUMO energy of -4.3 eV. BGTC OFET devices were all fabricated and tested in ambient condition. Unipolar electron mobilities as high as 0.9 $cm^2V^{-1}s^{-1}$ with an I_{on}/I_{off} of 10^5 were obtained. A device with an original electron mobility of ~0.35 $cm^2V^{-1}s^{-1}$ still showed a mobility of 0.18 $cm^2V^{-1}s^{-1}$ after storage in ambient air for 87 days.

In 2014 Zhang *et al.* expanded the π-surface of linear QOTs by using thieno[3,4-*b*]thiophene and 5-alkyl-4*H*-thieno[3,4-*c*]pyrrole-4,6(5*H*)-dione moieties to replace thiophenes.[73] The obtained 2D π-expanded QOTs with distal (**S22a**, **2DQTT-*o*)** and proximal (**S23a**, **2DQTT-*i***) regiochemistry (Figure 8) showed very small E_g^{opt} of 1.11 and 1.16 eV, respectively. The HOMO energies are -5.93 and -5.62 eV and the LUMO energies are very low at -4.51 and -4.77 eV for **S22a** and **S23a**, respectively. **S22a** underwent a dramatic redshift in its λ_{max} by 200 nm from solution to solid state, suggesting the formation of *J*-aggregates, which is favored for electron transport. On the other hand, **S21a** only showed a broader absorption profile with almost no change in its λ_{max} from solution to solid state. BGBC OFETs

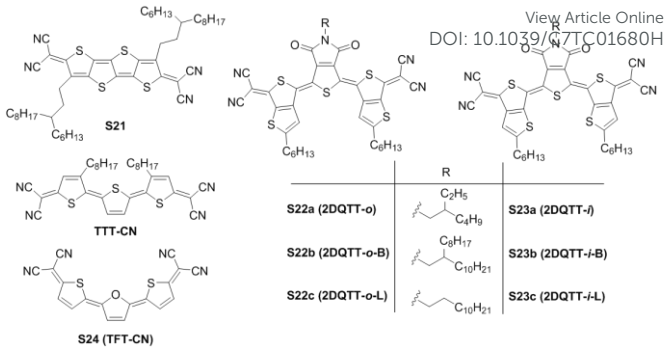

Figure 8. Dicyanomethylene-terminated quinoidal oligothiophenes (QOTs) with fused structures.

fabricated on octadecyltrichlorosilane (OTS)-modified SiO_2/Si substrates with 30 nm gold source and drain contacts were used to evaluate the semiconductors. The spin-coated semiconductor films (~40 − 60 nm) were annealed at 80, 120, 160, 190, or 240 °C. Devices were tested in ambient conditions and all devices showed n-type semiconductor performance. Devices based on **S23a** showed a maximum mobility of 0.44 $cm^2V^{-1}s^{-1}$ with an I_{on}/I_{off} of 10^3 at an annealing temperature of 190 °C. **S22a** based devices displayed the highest electron mobility of 3.0 $cm^2V^{-1}s^{-1}$ with I_{on}/I_{off} as high as 10^6 for the films annealed at 160 °C. The overall greater electron mobility observed for these 2D π-expanded QOTs compared to the linear QOTs was ascribed to the O−S and/or S−S intramolecular interactions and the favourable "brick-layer" arrangement in the solid state due to the expanded π-surface and steric hindrance that resulted in an exclusive *E*,*E*-configuration. The better performance of **S22a** than that of **S23a** was attributed to the formation of *J*-aggregates, higher crystallinity (verified by XRD), as well as larger grains (visualized by AFM) of the former. The results indicated that the orientation of the thieno[3,4-*b*]thiophene units has a huge impact on the molecular packing motif and electron transport. It should be noted that the $I_D^{1/2}$-V_{GS} curve of the **S22a** based devices showed a "kinked" nonlinear pattern and the mobilities were extracted from the low V_{GS} region. OFET devices based on **S22a** and **S23a** showed good air stability owing to their very deep LUMO energies.

Later, Zhang *et al*. reported another series of 2DQTT semiconductors, where the 2-ehtylhexyl side chains on the central 4*H*-thieno[3,4-*c*]pyrrole-4,6(5*H*)-dione moiety in **S22a** and **S23a** were replaced by either branched 2-octyldodecyl (**S22b** and **S23b**) or linear dodecyl (**S22c** and **S23c**).[74] Despite their different side chains, **S22b** and **S23c** have the same HOMO and LUMO energies of -5.59 and -4.44 eV and **S23b** and **S23c** have the same HOMO and LUMO levels of -5.57 and -4.54 eV, respectively. While **S23b** displayed the lowest electron mobility of ~0.1 $cm^2V^{-1}s^{-1}$, the linear alkyl substituted **S22c** and **S23c** showed much higher electron mobilities of 0.36 and 0.48 $cm^2V^{-1}s^{-1}$, respectively. A surprisingly high electron mobility of 5.2 $cm^2V^{-1}s^{-1}$ was achieved for **S22b**, which was attributed to its co-facial molecular packing forming a 2D brickwork motif that promotes π-overlap and 2D charge transport. In contrast, **S22c** formed a herringbone motif with edge-to-face orientation

View Article Online
DOI: 10.1039/C7TC01680H

(orthogonal) packing that can only promote 1D charge transport. Similar to **S22a**, the $I_D^{1/2}$–V_{GS} curves for the **S22b** and **S22c** are also kinked and the mobilities reported were the highest values in the low V_{GS} region. It is rather interesting to note that all compounds with the distal regiochemistry (2DQTT-*o*) showed the kinked $I_D^{1/2}$–V_{GS} curves while the compounds with the proximal (2DQTT-*i*) regiochemistry showed $I_D^{1/2}$–V_{GS} curves that fit the MOSFET model better. Further investigation into the influence of the regiochemistry of these series of compounds on the non-ideal OFET behaviour may be warranted.

A furan–thiophene quinoidal compound, **S24** (**TFT-CN**), was recently reported by Li *et al*.[75] It was found that **TFT-CN** existed as a *cis–cis* structure in the solid state, which is different from the all thiophene analogue (**TTT-CN**) that was previously reported to have a *trans–trans* structure in crystals.[96] **S24** has LUMO and HOMO energies of -4.15eV and -5.72 eV, respectively, which are only very slightly higher than those of **TTT-CN** (-4.22 eV/-5.74 eV). The spin coated **S24** films annealed at 150 °C exhibited remarkably high electron mobilities of up to 1.1 $cm^2V^{-1}s^{-1}$, while the corresponding **TTT-CN** based transistors showed much lower mobilities with a maximum value of 0.05 $cm^2V^{-1}s^{-1}$. The significant improvement in the mobility by incorporating a furan unit in **S24** was explained by the desirable molecular packing with the π-π stacking direction parallel to and the *c*-axis of the unit cell perpendicular to the substrate surface. In contrast, the **TTT-CN** films were comprised of two phase structures. When micro-ribbons of **S24** were used as the channel semiconductor to minimize the grain boundaries, electron mobilities as high as 7.7 $cm^2V^{-1}s^{-1}$ were achieved.

2.5. Isoindigo derivatives

The building blocks based on isoindigo and its derivatives are electron-deficient, which have recently been extensively studied for constructing high mobility n-type materials. In 2015 Xu *et al*. reported two isoindigo derivative **S25a** and **S25b** (Figure 9) based on the fusion of benzothiophene or benzofuran and isoindigo.[76] The LUMO energies of **S25a** and **S25b** are determined by CV measurements to be -3.72 eV and -3.73 eV, respectively. Under ambient conditions the spin coated **S25a** films exhibited n-channel dominant ambipolar charge transport performance with electron and hole mobilities of up to 0.011 $cm^2V^{-1}s^{-1}$ and 5.72 × 10^{-4} $cm^2V^{-1}s^{-1}$, respectively, in OFETs. On the other hand, **S25b** showed unipolar n-type semiconductor performance with higher electron mobilities of up to 0.074 $cm^2V^{-1}s^{-1}$. The better performance observed for **S25b** was explained by the higher crystallinity and better morphology (with less and smaller grain boundaries) than **S25a**.

(3*E*,7*E*)-3,7-Bis(2-oxoindolin-3-ylidene)benzo[1,2-*b*:4,5-*b*']difuran-2,6(3*H*,7*H*)-dione (IBDF)[97] (also termed as BDPPV,[98] BDOPV[78] or BIBDF[99]), which can be viewed as a fused ring structure formed through insertion of benzodifurandione into an isoindigo unit, has been recently discovered to be an excellent electron deficient building block for high mobility n-type small molecule and polymer semiconductors. A non-peripherally substituted BDOPV, **S26a**, has a LUMO energy of -3.64 eV and a HOMO of -5.98 eV.[77] Single crystals of **S26a**

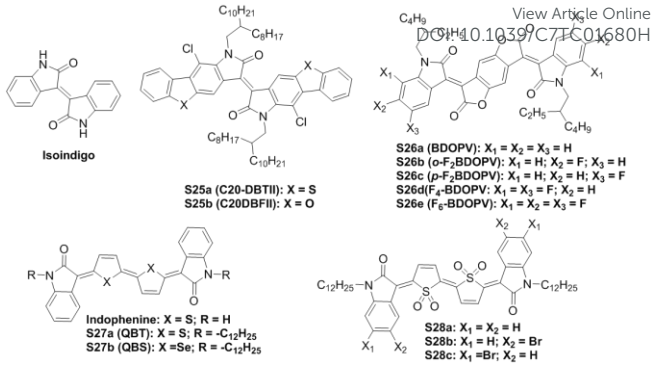

Figure 9. Isoindigo (IID) and its derivatives.

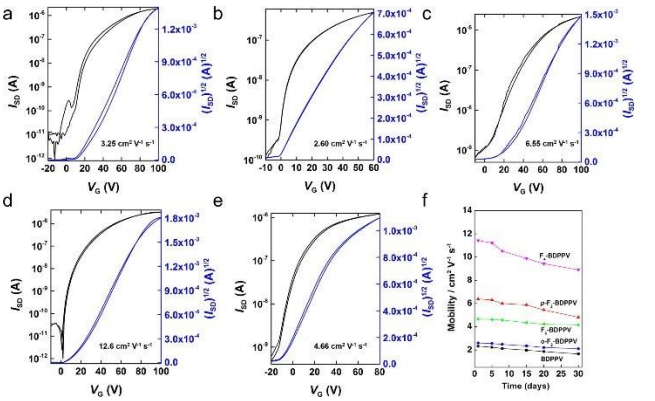

Figure 10. Transfer curves of OFETs based on (a) **S26a**, (b) **S26b**, (c) **S26c**, (d) **S26d**, and (e) **S26e**. (f) Stability of the devices in air at room temperature (RH = 50–60%). Reproduced with permission from ref 77. Copyright 2015 American Chemical Society.

showed unipolar n-type semiconductor performance with very high electron mobility of up to 3.25 $cm^2V^{-1}s^{-1}$ and I_{on}/I_{off} of >10^6 in OFETs. By substitution at the 6-postion of the indole moieties with fluorine atoms, the resulting tetra-fluorinated BDOPV, **S26b**, exhibited lower LUMO and HOMO energies of -3.84 eV and -6.18 eV, respective. Single crystals of **S26b** showed slightly lower electron mobilities of 2.60 $cm^2V^{-1}s^{-1}$ than those of **S26a**. When the fluorine substitution was at the 5-positions of the indole moieties, the product **S26c** displayed similar LUMO and HOMO energies (-3.84 eV and -6.13 eV) as those of **S26b**. However, this compound exhibited much higher electron mobilities of up to 6.55 $cm^2V^{-1}s^{-1}$. When both 5- and 6-positions were substituted with fluorine atoms, the tetrafluorinated product **S26d** showed deeper LUMO and HOMO energies of -4.03 eV and -6.32 eV, respectively. Ultrahigh electron mobilities of up to 12.6 $cm^2V^{-1}s^{-1}$ were achieved for the devices with single crystal **S26d** in TGBC OFETs.[78] The high electron transport performance of this molecule was interpreted by its antiparallel cofacial packing in the single crystal, which generates a large charge transfer integral along the π–π stacking direction. Further increasing the fluorine substituents to six, the resulting **S26e** has even lower LUMO and HOMO energies of -4.10 eV and -6.40 eV, respectively.[77] However, the electron mobilities of this compound dropped with the highest value of 4.66 $cm^2V^{-1}s^{-1}$. All devices based on these series of compounds showed less than

20% degradation when kept in ambient air (relative humidity, RH = 50–60%) for 30 days (Figure 10).

Indophenine has a quinoidal bithiophene core flanked by two indole units, which was first reported by Baeyer in 1879 and has been used as blue dyestuff since.[100] Hwang *et al.* synthesized soluble *N*-dodecyl substituted indophenine, **S27a** (**QBT)**, and a biselenophene analogue, **S27b** (**QBS)**.[79] Both compounds showed ambipolar charge transport performance in OFETs due to their relatively low LUMO (-3.76 eV for **S27a** and -3.73 eV for **S27b**) and high HOMO (-5.25 eV for **S27b** and -5.33 eV for **S27b**) energies that facilitate the injection and transport of both electrons and holes. The electron and hole mobilities are ~10^{-3}–10^{-2} $cm^2V^{-1}s^{-1}$ for both compounds with **S27b** performing slightly better. To further lower the energy levels in order to realize unipolar n-type semiconductor performance, Deng *et al*. recently successfully oxidized the sulphur atoms in the thiophene units of *N*-dodecyl substituted indophenines to prepare a series of thiophene-*S*,*S*-dioxidized indophenine (IDTO) compounds, **S28a**, **S28b**, and **S28c**.[80] The LUMO and HOMO energies of **S28a** are significantly lowered to -3.99 eV and -5.85 eV, respectively. The 5- and 6-bromo substituted compound, **S28b** and **S28c**, showed even lower LUMO (-4.12 eV and –4.18 eV, respectively) and HOMO (-6.33 eV and -6.30 eV, respectively) energies. As a result, all three IDTO compounds exhibited unipolar n-type semiconductor performance in OFETs with Au contacts. **S28a** showed electron mobilities of up to 0.04 $cm^2V^{-1}s^{-1}$ in OFETs. **S28b** showed improved mobilities of up to 0.07 $cm^2v^{-1}s^{-1}$. The highest electron mobility of 0.11 $cm^2V^{-1}s^{-1}$ was achieved for **S28c**. It should be noted that **S27a** and **S27b** are each a mixture of inseparable six isomers. By introducing oxygen atoms on thiophenes, **S28a**, **S28b**, and **S28c** only consisted of the pure (*E*,*E*,*E*) isomers after heating at a moderate temperature of ~100 °C, suggesting that the incorporated oxygen atoms on thiophenes may exert some steric effect to prevent the formation of other isomers. Therefore, in addition to the lowered LUMO energy, the existence of a single isomer might also contribute to the higher electron mobilities of **S28** than those of **S27**.

3. Polymeric n-type semiconductors

3.1. Rylene diimide-based polymers

Among various n-type rylene diimide-based polymers reported in the past few years, NDI-based copolymers are the most studied for various applications including OFETs and OPVs.[41,101] The best known n-type polymer, poly {[*N*,*N*'- bis(2-octyldodecyl)-naphthalene-1,4,5,8-bis(dicarboximide)-2,6-diyl]-alt-5,5'-(2,2'-bithiophene)} (**P1a**, **P(NDI2OD-T2)**, in Figure 11), also known as N2200, was first reported by Watson *et al.* [102] in 2008 and was later studied for n-channel OTFTs by Fachetti, Watson, Jenekhe, *et al*. [103,31,104,105] **P1a** has been the most extensively investigated n-type polymer for OFETs and all-polymer solar cells to date.[106–110] **P1a** has a low LUMO energy of ca. -4 eV, which is sufficient for achieving stable electron transport. **P1a** showed n-type semiconductor performance with high electron mobilities of up to 0.85 $cm^2V^{-1}s^{-1}$ in TGBC devices and ~0.2 $cm^2V^{-1}s^{-1}$ in BGTC devices when measured under ambient conditions.[31] TGBC devices showed almost no change in performance after stored in air for up to 30 weeks, while the BGTC devices were less stable. Several strategies have been adopted aiming to improve the performance of this polymer in

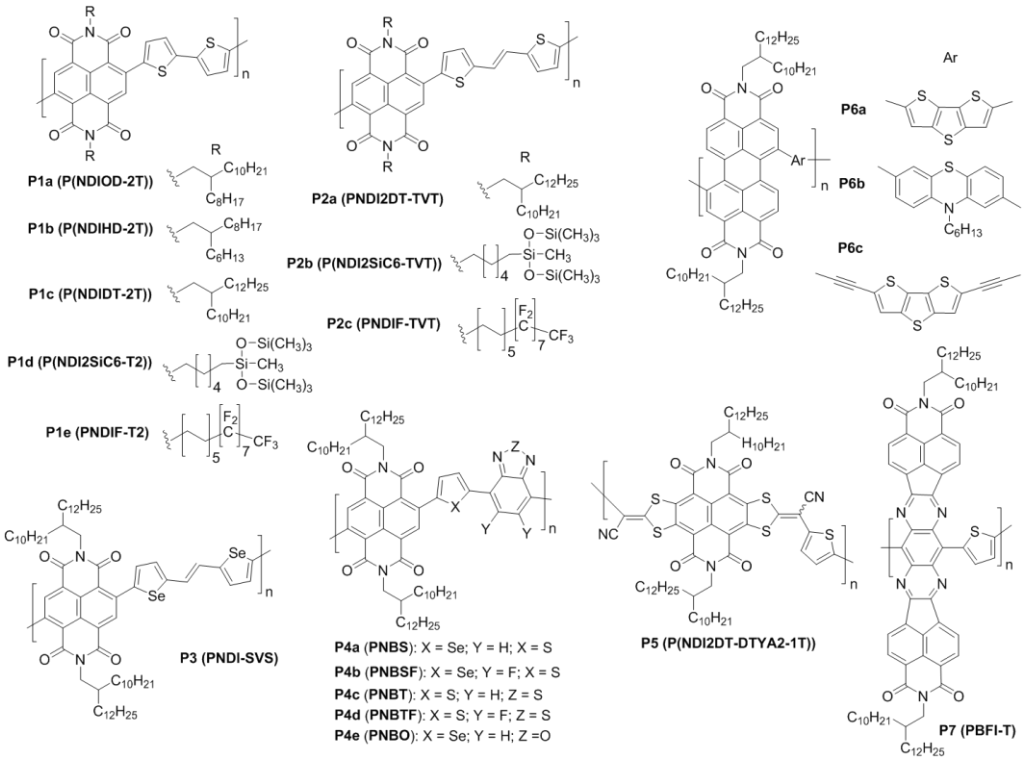

Figure 11. Rylene diimide-based polymers.

View Article Online
DOI: 10.1039/C7TC01680H

Compound	Acronym	E_{LUMO}/E_{HOMO}, ev	Device structure-source-drain material/deposition method (SX: single crystal; VD: vacuum deposition; SP: spin coating; SD: drop coating	μ_e or μ_e/μ_h, $cm^2V^{-1}s^{-1}$	I_{on}/I_{off}	V_{th}, V	Test atm.	% of initial μ_e/ storage time in ambient air	Year [Ref.]
P1a	**P(NDI2OD-T2)**	-3.91/-5.36 [103]	TGBC-Au /SP BGTC-Au /SP BGTC-Au/DC	0.85 0.2 1.22	10^6-10^7 10^5	5–20 41.66	air air N_2	100%/30w ~20%/16 w [103]	2009 [31] 2009 [31] 2016 [111]
P1b	**P(NDI2HD-T2)**		BGTC-Au/DC	1.90	10^4	35.9	N_2		2016 [111]
P1c	**P(NDI2DT-T2)**		BGTC-Au/DC	0.39	10^4	34.8	N_2		2016 [111]
P1d	**P(NDI2SiC6-T2)**	-3.83/-5.27	TGBC-Au/SP	1.04	10^3	21.6	N_2		2015 [112]
P1e	**PNDIF-T2**	-4.01/-5.62	BGTC-Au/SP BGTC-Au/CN-SP[a]	3.93 6.5	10^5	7.3 14.4	air	100%/3mo	2016 [113]
P2a	**PNDI2DT-TVT**	-4.00/-5.42	TGBC-Au/SP TGBC-Cs_2CO_3-Au/SP	1.4/0.14 1.80	10^3/10 10^6	9.89/-72 12.60	N_2		2013 [114]
P2b	**P(NDI2SiC6-TVT)**	-3.96/-5.36	TGBC-Au/SP	0.93	10^3	33.6	N_2		2015 [112]
P2c	**PNDIF-TVT**	-3.99/-5.38	BGTC-Au/SP BGTC-Au/CN-SP[a]	3.75 5.64	10^5 10^5	18.3 14.7	air	100%/3mo	2016 [113]
P3	**PNDI-SVS**	-3.98/-5.29	TGBC-Au-SD/SP TGBC-Au/Cs_2CO_3-SD/SP	2.4/(amibi) 0.5	10^3 10^4	14.6	N_2		2016 [115]
P4a	**PNBS**	-3.77/-5.84	TGBC-Au-SD/SP	8.5/1.7		57/-75	air	~100/100d	2017 [116]
P4b	**PNBSF**	-3.85/-6.24	TGBC-Au-SD/SP	3.5		48	air		2017 [116]
P4c	**PNBT**	-3.81/-5.90	TGBC-Au-SD/SP	3.1/0.7		38	air	~100/100d	2017 [116]
P4d	**PNBTF**	-3.88/-6.20	TGBC-Au-SD/SP	2.2		60	air		2017 [116]
P4e	**PNBO**	-3.98/-5.90	TGBC-Au-SD/SP	2.43	10^3	42	air	~100/70d	2017 [117]
P5	**P(NDI2DT-DTYA2-1T)**	-4.25/-5.82	BGBC-Au/SP	0.38	10^6	-4.32	N_2		2014 [118]
P6a		-3.9/-5.9	BGTC-Al/SP	0.013	10^4		N_2		2007 [119,120]
P6b	**PPP24-H**	-3.7/-5.8	BGTC-Al/SP	0.05	10^5	8	N_2		2012 [121]
P6c		-4.0/-5.8	BGBC-Au/SP	0.075			Air	45% /6d	2013 [122]
P7	**PBFI-T**	-3.80/-5.45	BGTC-Ag/SP	0.30			N_2		2013 [123]
P8a	**PDBT-HD**	-3.68/-5.40	BGTC-Au/SP	0.057/0.024			N_2		2012 [124]
P8b	**N-CS2DPP-OD-TEG**	-3.66/-5.38	BGBC-Au/SP TGBC-Al-Au/SP	0.01/0.01 3	 10^4		N_2		2012 [125]
P9	**PDPP-TBT**	-4.0/-5.2	BGTC-Au/SP	0.40/0.35			N_2		2010 [126]
P10	**PDBTAZ**	-4.24/-5.67	TGBC-Au/SP TGBC-Au-PEI/SP TGBC-Au/PEI-SP	0.41/0.36 0.53 0.88	 10^4 10^3-10^4	 21	N_2		2012 [127] 2014 [128] 2015 [129]
P11	**PDPPTPT-CN**	-3.71/-5.63	BGTC-Au-SD/SP	0.18/ 8.6×10^{-3}	10^2/10^3	45/-55	air		2015 [130]
P12a	**PDBTz**	-3.75/-5.54	BGTC-Ag/Al/SP TGBC, Ag-PEIE/SP[b]	0.21 0.31	10^5 10^5	7.8 4.0	air (RH=55-60%)	75%/5mo	2015 [131]
P12b	**PDBTz**	-3.63/-5.56	TGBC-Au/SP	0.53/5.9×10^{-2}	10^5/10^6		N_2		2016 [132]
P13	**PDPP4Tz**	ca. -3.9~-4.1/-5.71	BGBC-/SP	0.07	10^5		N_2	100% (tested in N_2)/4 mo (RH=55-60%)	2016 [133]
P14	**PDBPyBT**	-4.33/-5.69	TGBC-Au-SD/SP TGBC-Au-PEI/ SP[c] TGBC-Au/PEI-SP[d]	6.30/2.78 1.42 0.95	10^3/10^3 10^3 10^3	 4	N_2		2014 [134] 2014 [128] 2015 [129]
P15	**PDBPyTT**	-4.3/-5.7	TGBC-Au/SP TGBC-Au-PEI/SP[c]	3.36/2.04 2.38/0.20	 10^3	 5/10	N_2		2015 [135]
P16	**PAIID-BT-C3**	-3.64/-5.67	BGBC-Au/SP TGBC-Au/SP	-/7.28 0.78/2.33			air		2016 [136]
P17	**PAIIDSe**	-4.0/-5.6	TGBC/SP	0.5/0.2			N_2		2016 [137]
P18	**PAIIDBT**	-4.1/-5.8	TGBC/SP	1.0	10^6		N_2		2016 [137]
P19	**PIBDF-T**	-4.43/-5.79	BGBC-Au/SP	5.4×10^{-3} 8.2×10^{-3}/1.0×10^{-2}	10^4		N_2 air		2013 [97]
P20b	**BDOPV-2T**	-4.15/-5.72	TGBC-Au/SP	1.74	10^4~10^5	44	air (RH=40-50%)	22%/15d	2013 [138]
P20c	**PIBDFBT-37**	-3.87/-5.72	BGBC-Au/SP	0.35/0.20			N_2		2015 [139]
P21	**F_4BDOPV-2T**	-4.32/-5.96	TGBC-Au/SP	14.9 (1.24)[e]	10^3-10^4	-17	air (RH=50-60%) (30 days)	60%/30d	2016 [23]
P22	**AzaBDOPV-2T**	-4.37/-5.80	TGBC-Au/SP	3.22	10^4-10^5		air (RH=50-60%)		2016 [140]
P23	**BDOPV–TT**	-3.88/-5.70	TGBC-Au/SP	1.37/1.70		33/-65	air (70 days)	50%/70d	2015 [141]
P24	**BDPPV**	-4.10/-6.12	TGBC-Au/SP	1.1	10^5	5	air (30 days)	30%/30d	2013 [98]
P25	**PIDTOTT**	-3.98/-5.92	BGBC-Au/SP	0.14	10^4	1.8	N_2		2016 [142]
P26	**PIDTOBT**	-4.09/-5.78	BGBC-Au-SD/SP	0.18	10^5	2.3	N_2		2016 [143]

[a]Chloronaphthalene (CN) was added as a solvent additive. [b]PEIE modified source and drain. [c]PEI modified source and drain. [d]Polymer is n-doped with PEI. [e]Values are obtained in low (high) V_G region.

Table 2 Summary of properties of n-type polymer semiconductors.

OFETs. Among them, side chain engineering is proven a very effective approach. Lee *et al*.[111] synthesized a series of NDI-bithiophene-based copolymers (P(NDIR-T2)) with different alkyl side chains, 2-hexyldecyl (2-HD) (**P1b**), 2-octyldodecyl (2-OD) (**P1a**), and 2-decyltetradecyl (2-DT) (**P1c**), which showed notable differences in their morphology, crystalline structures, and ultimately charge transport performance. They found that the electron mobility of these polymers in BGTC OFETs increases with the shortening of the alkyl side chains. The highest mobility of 1.90 $cm^2V^{-1}s^{-1}$ was achieved for **P1b**, which is much higher than those of **P1a** (1.22 $cm^2V^{-1}s^{-1}$) and **P1c** (0.39 $cm^2V^{-1}s^{-1}$). The improved mobility of **P1b** was explained by the shorter intermolecular π-π distance of this polymer compared with the other two, which facilitated the interchain charge hopping.

The hybrid siloxane terminated side chains were used for p-type isoindigo polymers and an enhancement in the hole mobility was observed.[144] Kim *et al*. incorporated the hybrid siloxane-terminated hexyl chain (SiC_6) to NDI to form **P(NDI2SiC6-T2)** (**P1d**).[112] **P1d** showed much better mobility of 1.04 $cm^2V^{-1}s^{-1}$ than that of the benchmark **P1a** (0.32 $cm^2V^{-1}s^{-1}$) in OFETS fabricated and tested under same conditions. The XRD results revealed that in **P1d** the polymer chains formed quite balanced face-on and edge-on orientations rather than one preferred orientation. In addition, **P1d** exhibited much stronger π-π stacking interaction evidenced by its stronger (010) diffraction peak. These factors might have contributed to its enhanced charge transport performance compared to **P1a**.

Kang *et al*. synthesized another NDI-T2 polymer, **P1e**, with semifluoroalkyl ($-(CH_2)_5(CF_2)_7CF_3$) side chains to replace hydrocarbon side chains.[113] BGTC OFETs using spin coated polymer films with chloroform as a solvent exhibited high electron mobility of 3.93 $cm^2V^{-1}s^{-1}$. Devices showed no obvious degradation in performance after exposure to air for three months. With the addition of a higher boiling point additive, 1-chloronaphthalene, to the solvent, the obtained polymer films showed even high electron mobilities of up to 6.5 $cm^2V^{-1}s^{-1}$, owing to the improved chain packing. Two-dimensional grazing-incidence X-ray diffraction (2D GIXD) data (Figure 12) indicated that the **P1e** film showed intense (00l) reflections along the in-plane direction, while **P1a** with branched alkyl side chains showed no corresponding reflections. It was believed that the introduction of the semifluoroalkyl side chains in **P1e** can make the polymer backbone more rigid and strengthen the self-organization of the side chains themselves, forming a superstructure composed of "backbone crystals" and "side-chain crystals". The rigid backbone organization was considered to be mainly responsible for the enhanced charge transport of **P1e**. The AFM images of these two polymers also showed distinct differences. The **P1a** film had small irregular grains, while the **P1e** film was consisted of much larger, elongated grains with better connectivity (shown in Figure 12 and in the Supporting Information of paper).[113] However, this polymer showed slight hole transport behaviour with hole mobilities two orders of magnitude lower than the electron mobilities.

Efforts have also been made to alter the bithiophene donor unit in NDI-T2 to thiophene-vinylene-thiophene (TVT) since the use of TVT has met successes in other types of polymers. TVT

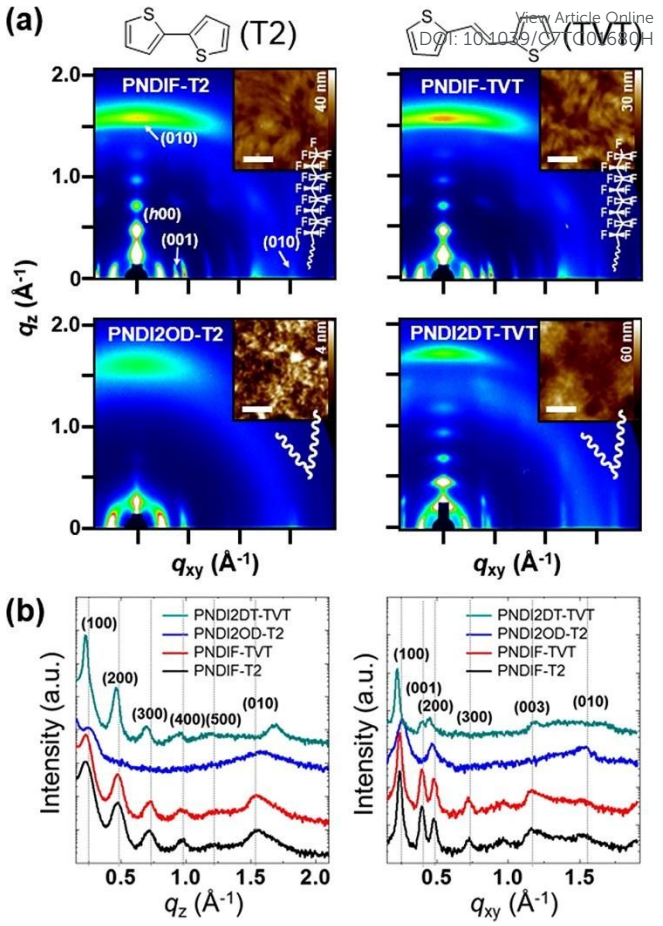

Figure 12. (a) 2D GIXD patterns of thin films of **P1e** (**PNDIF-T2**), **P2c (PNDIF-TVT, P1a** (**PNDI2OD-T2**) and **P2a**(**PNDI2DT-TVT**) thermally annealed at 250 °C. The insets are the AFM height images of the corresponding thin films, where the scale bars are 500 nm. (b) The corresponding GIXD diffractogram profiles along the out-of-plane and in-plane directions. Reproduced with permission from ref. 113. Copyright 2016 American Chemical Society.

has a highly coplanar structure, which can facilitate the polymer main chain packing and reduce the π-π stacking distance.[145] An NDI-TVT polymer with 2-decyltetradecyl side chains, **P2a**, was reported by Kim *et al*.[114] Incorporation of TVT raised the HOMO energy to -5.42 eV, but the LUMO energy remained similar at -4.0 eV compared to the NDI-T2 polymer, **P1a**. As a result, ambipolar charge transport was observed for **P2a** in OFETs with Au as contacts. When Cs_2CO_3 was used to modify the Au contact surface to reduce the work function, unipolar electron transport was achieved due to the increased hole injection barrier. High electron mobility of up to 1.8 $cm^2V^{-1}s^{-1}$ was obtained. The improved charge transport was attributed to the improved π-π intermolecular interaction. The devices also showed good air and bias stress stabilities. Side chain engineering was also conducted on NDI-TVT polymers. With the hybrid siloxane terminated hexyl (SiC_6) side chains, **P2b** showed a highest electron mobility of 0.93 $cm^2V^{-1}s^{-1}$,[112] which is better than that of **P1a**, but lower than that of its corresponding NDI-TVT polymer **P2a**. Kang *et al*. prepared an NDI-TVT polymer **P2c** with semifluoroalkyl ($-(CH_2)_5(CF_2)_7CF_3$) hexyl side chains on NDI to make **P2c**.[113] **P2c** showed good solubility in some common organic solvents such as chloroform and chlorobenzene. As with **P1e**, it was also found that these side chains improved the

View Article Online DOI: 10.1039/C7TC01680H

packing of the rigid polymer backbone evidenced by the 2D-GIXD and AFN data (Figure 12). Very high electron mobility of up to 5.64 $cm^2V^{-1}s^{-1}$ was obtained for in TGBC devices with polymer films processed using chloroform as the solvent with the aid of a solvent additive, 1-chloronaphthalene. The transistor performance was almost unchanged in ambient air after three months.

Selenophene-vinylene-selenophene (SVS) has been used as a donor unit and produced some of the best performing p-type polymer semiconductors such as a DPP-SVS polymer, which demonstrated an ultrahigh mobility of ~12 $cm^2V^{-1}s^{-1}$.[21] Very recently, SVS was used as the donor unit to form an NDI-SVS polymer, **P3**.[115] The HOMO energy increased to -5.29 eV, while the LUMO energy kept similar at -3.98 eV in comparison to **P2a**. High electron mobilities of up to 2.4 $cm^2V^{-1}s^{-1}$ were achieved in TGBC OFETs with **P3** films spin coated and annealed at 250 °C, better than that of its NDI-TVT counterpart **P2a** (1.8 $cm^2V^{-1}s^{-1}$). However, **P3** also showed hole transport performance due to its high HOMO energy, which facilitates the hole injection and transport. By introducing a thin Cs_2CO_3 layer between the Au source/drain and the semiconductor layer, unipolar n-type OFET performance with electron mobility of up to 0.5 $cm^2V^{-1}s^{-1}$ was realized for the as-cast polymer films.

Recently, Zhao *et al*.[116] used the comonomer blocks, selenophene-benzothiadiazole-selenophene and thiophene-benzothiadiazole-thiophene, to make a series of NDI polymers, **P4a-d** (Figure 11). The incorporation of the weak acceptor benzothiadiazole aimed to fine-tune the electronic structure and thus the charge transport property of the polymer. **P4a** and **P4b** with selenophene as the donor units exhibited much higher electron mobilities than **P4c** and **P4d** that have thiophene donors, which was explained by the much better film forming ability of **P4a** and **P4b** due to the presence of selenophene. The highest electron mobility of 8.5 $cm^2V^{-1}s^{-1}$ among these series was achieved for **P4a** in a TGBC device. **P4a** and **P4c**, which have LUMO/HOMO energies of -3.77 eV/-5.84 eV and -3.81 eV/-5.90 eV, showed ambipolar charge transport performance. By incorporating two fluoro substituents to benzothiadiazole, the resulting **P4b** and **P4d** showed slightly lower LUMO energies of -3.85 eV and 3.88 eV as well as much lower HOMO energies of -6.20 eV and -6.24 eV, respectively. The fluoro substitution on the benzothiadiazole seems mainly contributed to the lowering of the HOMO energies, which would build up higher energy barriers for hole injection. As a result, these two polymers showed unipolar n-type semiconductor performance with the maximum electron mobilities of 3.5 and 2.2 $cm^2V^{-1}s^{-1}$, respectively, which are lower than their corresponding non-fluoro counterparts, **P4a** and **P4c**. The lower solubility and thus poor film quality of **P4b** and **P4d** might be contributed to their poor performance. The TGBC devices of **P4a** and **P4c** showed excellent stability in air. After 100 days in air, the devices showed negligible changes in performance. In the BGBC devices, all the polymers showed much lower performance with electron mobilities in the range of 0.15-0.29 $cm^2V^{-1}s^{-1}$ when tested in a N_2-filled glove box. Significant decreases in hole and electron mobilities were observed after the devices were exposed to ambient air for two hours. The same group reported a similar polymer, **P4e**, which contains a selenophene-benzooxadiazole-selenophene.[117] This polymer has a lower LUMO energy of -3.98 eV together with a low HOMO energy of -5.90 eV, which enabled a unipolar electron-transport characteristics of this polymer in OFETs. The TGBC devices showed no obvious decay in performance after being stored in air for 70 days. The air stability of this polymer in bottom gate devices was not reported.

A core-extended NDI moiety has also been incorporated into a polymer backbone of **P5**, which has low HOMO and LUMO energies of -5.82 eV and -4.25 eV, respectively.[118] At an optimized temperature of 120 °C, an electron mobility of 0.38 $cm^2V^{-1}s^{-1}$ with a high I_{on}/I_{off} of 10^6 was achieved in BGBC devices.

Another rylene diimide building block, PDI, has also gained considerable attention as it has demonstrated gradual improvement in performance in both OFETs and OPVs.[146] The initially reported PDI-based polymer, **P6a**, exhibited modest unipolar electron mobilities of up to 1.3×10^{-2} $cm^2V^{-1}s^{-1}$.[119,120] Marked improvements were later reported with the inclusion of a phenothiazine comonomer, **P6b**, with electron mobilities approaching 0.05 $cm^2V^{-1}s^{-1}$ with I_{on}/I_{off} of 10^5 for devices measured in nitrogen.[121] By introducing acetylene linkages, the resulting polymer **P6c** has a lower LUMO energy and a higher HOMO energy than those of **P6a** without the acetylene linkages, due to the more coplanar structure and thus more extended conjugation of the former.[122] Increased electron mobility of up to 0.075 $cm^2V^{-1}s^{-1}$ with I_{on}/I_{off} of 10^6 were achieved. More importantly, due to the lowered LUMO energy of **P6c**, the devices showed good stability in ambient air with 45% retention of the mobility after being stored in air for 6 days.

A tetraazabenzodifluoranthene diimide based polymer, **P7**, reported by Jenekhe *et al*. has two-dimensional π-conjugation in parallel and normal to the main chain.[123] XRD analysis revealed that the polymer chains in the drop cast films adopted a lamellar packing motif with a very short π-π distance of 0.35 nm, which would facilitate the charge transport in the third dimension (the π-stacking direction). High electron mobilities of up to 0.30 $cm^2V^{-1}s^{-1}$ were achieved in BGTC devices with Ag contacts in nitrogen for the films annealed at 200 °C. The LUMO energy of this polymer, -3.8 eV, seems insufficient for achieving air stability of the operating devices with this polymer.

3.2. DPP polymers

Diketopyrrolopyrrole (DPP) is a strong electron acceptor building block and some DPP based polymers represent the best performing polymer semiconductors for OFETs,[11,21] although the high mobility values obtained for some DPP polymers were thought to be overestimated[36] because their $|I_D|^{1/2}$–V_{GS} curves exhibited nonlinear kinks (as illustrated in Figure 3B). A DPP compound prepared by the common synthetic routes is accompanied by two flanking aromatic units. Thiophene is the mostly used flanking units to DPP because of its small steric effect that can keep the DPP2T (or DBT) structure highly coplanar, a feature that is desirable for achieving high carrier mobility. However, the electron donating effect of the flanking thiophene units raises the HOMO energy. Therefore, the polymers with the DBT backbone, e.g., **P8a**[124] and **P8b**[125] (Figure

View Article Online
DOI: 10.1039/C7TC01680H

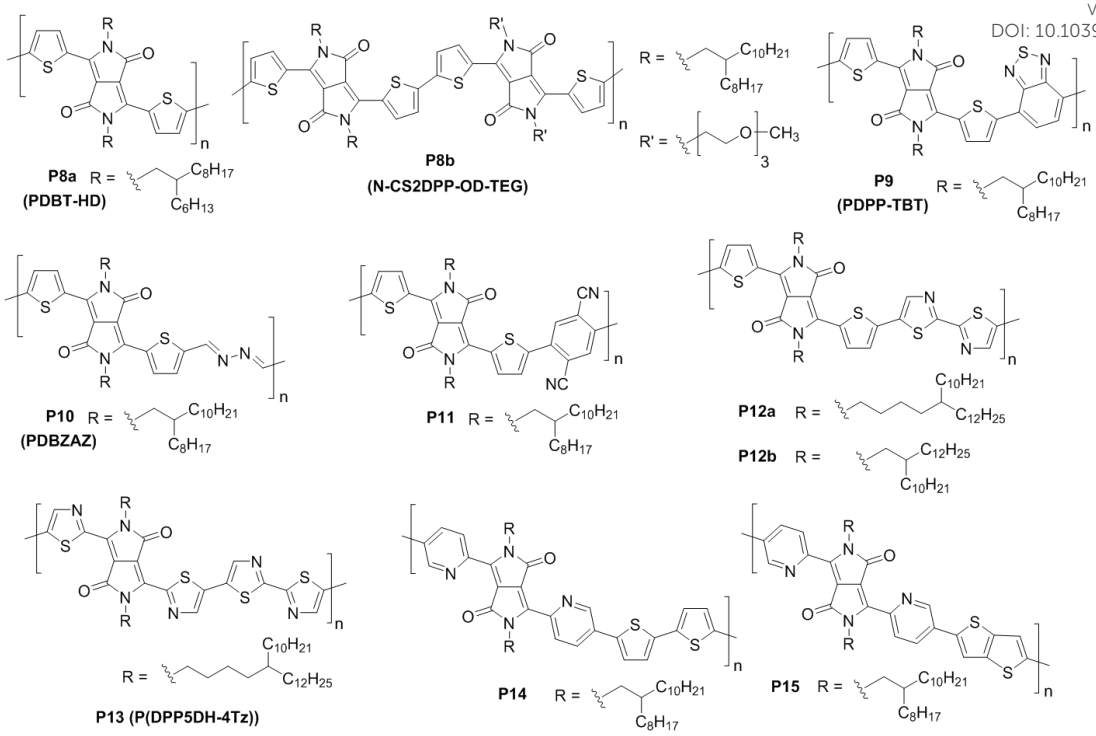

Figure 13. Diketopyrrolopyrrole (DPP)-based polymers.

13), have a rather high HOMO energy of -5.4 eV, although their LUMO energy of -3.7 eV is sufficiently low for stable electron transport. Thus, **P8a** and **P8b** exhibited ambipolar charge transport performance with quite balanced electron and hole mobilities on the order of 10^{-2} $cm^2V^{-1}s^{-1}$ in BGTC or BGBC devices when Au was used as source and drain contacts. When a TGBC structure with unsymmetrical contacts, Al as the source and Au as the drain, was used, unipolar n-type semiconductor performance with high electron mobilities of up to 3 $cm^2V^{-1}s^{-1}$ were obtained for **P8b**.[125] This is mainly due to the low work function of Al, which would block the hole injection and facilitate the electron injection. The fluorine polymer Cytop used as dielectric material might also be helpful for reducing the electron traps compared to the SiO_2 dielectric used in the bottom gate devices where the residue of Si-OH groups might serve as electron traps. Combining DPP2T with an electron acceptor comonomer benzothiadiazole unit led to a copolymer **P9**,[126] which showed a lower LUMO energy of -4.0 eV, but a higher HOMO energy of -5.2 eV compared to **P8**. This polymer showed ambipolar charge transport with high and balanced electron and hole mobilities of up to 0.40 $cm^2V^{-1}s^{-1}$ and 0.35 $cm^2V^{-1}s^{-1}$, respectively. The large fused benzothiadiazole spacer might strengthen the π-π interaction and increase the π-π overlapping, which are beneficial for the interchain charge transport along the π-stacks.

In order to promote the electron transport, Hong *et al*. used an electron deficient azine (C=N–N=C) unit to link DPP2T units through a convenient catalyst-free Schiff base type polymerization.[127] The formed polymer **P10** (**PDBTAZ**) showed a very low LUMO energy of -4.24 eV and a slightly lower HOMO energy of -5.34 eV compared to most DPP2T-donor type copolymers. **P10** showed good electron transport property with the highest electron mobility of 0.41 $cm^2V^{-1}s^{-1}$. However, similar hole mobilities of up to 0.36 $cm^2V^{-1}s^{-1}$ were also observed. Since Au was used as the contact material, the HOMO energy of this polymer would be inadequately low to block the hole injection.

Another electron withdrawing comonomer unit, dicyacypenylene, was used by Xiong *et al*.[130] to form a polymer **P11**. This polymer has a very low HOMO energy of -5.63 eV and yet a relatively low LUMO energy of -3.71 eV. The OFET devices showed good electron transport performance with electron mobilities of up to 0.18 $cm^2V^{-1}s^{-1}$. The lowered HOMO energy could build a larger hole injection barrier; however, weak hole transport (with hole mobility of 8.6×10^{-3} $cm^2V^{-1}s^{-1}$) was still observed.

Reichmanis *et al*. used the electron deficient bithiazole as the comonomer unit to DPP2T.[131] The polymer **P12a** showed a highest electron mobility of 0.3 $cm^2V^{-1}s^{-1}$ in OFETs, where low work function Ca and polyethylenimine ethoxylated (PEIE)-modified Ag were used as contact electrodes in BGTC and TGBC devices, respectively, in order to facilitate the electron injection. The use of these low work function contacts also had an effect on the blocking of hole injection, thus realizing the observed unipolar n-type semiconductor performance of this polymer. A similar polymer **P12b** reported by Guo *et al*.[132] showed n-type-dominant ambipolar charge transport performance in TGBC OFETs with the high work function Au as contacts. **P12b** showed better electron mobilities of up to 0.53 $cm^2V^{-1}s^{-1}$ along with hole mobilities of up to 4.8×10^{-2} $cm^2V^{-1}s^{-1}$. The improved electron mobility of **P12b** compared to **P12a** might be due to their different monomers and polymerization methods, direct arylation for **P12b** and Stille coupling for **P12a**,

View Article Online DOI: 10.1039/C7TC01680H

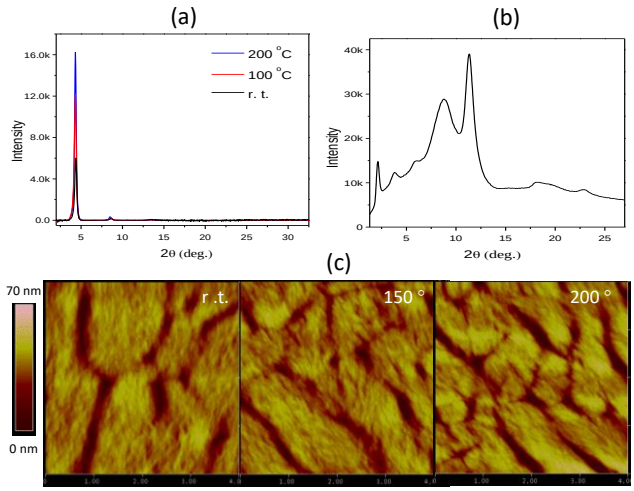

Figure 14. (a) XRD patterns of spin coated **P14** thin films on bare SiO_2/Si substrates annealed at different annealing temperatures measured in a reflection mode using Cu Kα1 radiation. (b) XRD pattern of a stack of non-annealed **P14** thin films in a transmission mode using Mo Kα radiation. (c) AFM images (2μm × 2μm each) of **P14** thin films on bare SiO_2/Si substrates annealed at different temperatures. Reproduced with permission from ref. 134. Copyright 2014 John Wiley & Sons.

which led to different types and amounts of structural defects in these two polymers. With a replacement of the flanking thiophenes to the DPP unit with thiazoles, the polymer **P13** exhibited unipolar electron mobilities as high as 0.067 $cm^2V^{-1}s^{-1}$ with modest I_{on}/I_{off} of 10^4-10^5 in BGBC devices with Au contacts when measured in nitrogen.[133] The electron affinity (EA) of this polymer was estimated to be between 3.9 eV and 4.1 eV, using the ionization potential (IP = 5.71 eV) measured by UPS and the band gap (1.34 eV) measured by UV-Vis. The high IP or low HOMO energy of this polymer would block the hole injection. To evaluate air stability, devices were stored in ambient air (25 °C and 50−60% RH) and characterized periodically in nitrogen by removing the absorbed air under a vacuum before the measurement. Devices showed no appreciable degradation in performance after 4 months, indicating the good air stability of the devices owing to the high IP/EA values of this polymer.

Sun *et al*. replaced the electron rich thiophene units in DPP2T with the electron deficient 2-pyridine units.[134] The connection of DPP to the 2-positions of the pyridine units is crucial to maintain the high coplanarity of the DPP2Py (or DBPy) building block. The copolymer of DPP2Py and bithiophene, **P14**, has LUMO and HOMO energies of -4.33 eV and -5.69 eV, respectively, which are much lower than those of the corresponding polymer using DPP2T, PDQT.[147] **P14** showed a very high electron mobility of 6.3 $cm^2V^{-1}s^{-1}$ in TGBC OFETs. The very high electron mobility achieved by **P14** was accounted mainly for by the extremely high crystallinity, which was verified by the intense X-ray diffraction peaks as well as the large crystalline domains shown in the AFM image of the spin coated polymer film (Figure 14). While the very low LUMO energy of **P14** is very beneficial for the electron injection and transport, the HOMO energy of -5.69 eV seems insufficient to block the hole injection when Au, which has a work function of ~5.1 eV. Therefore, high hole mobilities of up to 2.78 $cm^2V^{-1}s^{-1}$ were also observed. Another copolymer of DPP2Py with thieno[3.2-*b*]thiophene, **P15**,[135] showed similar LUMO and HOMO energies

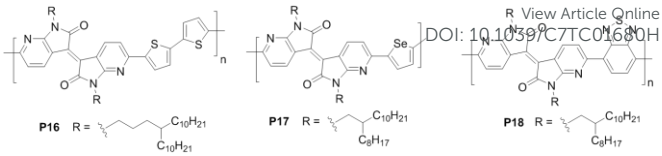

Figure 15. Diazaisoindigo (AIID) based polymers.

as those of **P14**. With pure Au contacts, the TGBC OFETs with **P15** showed high electron and hole mobilities of 3.36 $cm^2V^{-1}s^{-1}$ and 2.04 $cm^2V^{-1}s^{-1}$, respectively. To block the hole injection, a thin layer of polyethylenimine (PEI) was used to modify the Au contact surface, which led to a reduction of the work function of the electrode down to 3.2 eV. With the PEI modified Au contacts, unipolar n-type semiconductor performance was realized. High electron mobility of up to 2.38 $cm^2V^{-1}s^{-1}$ was achieved. Surface modification of the contact electrodes by PEI was also proven a simple and versatile approach to converting ambipolar OFETs to unipolar n-channel OFETs for several other ambipolar polymers.[128]

3.3. Isoindigo derivatives based polymers

Isoindigo (IID) is an electron acceptor building block and the D-A polymers based IID have achieved high hole mobilities in OFETs.[148] However, the electron affinity of IID is insufficient to bring down the LUMO energy low enough to achieve stable electron transport characteristics. Huang *et al*. replaced the benzene ring in IID with the more electron-withdrawing pyridine to form 7,7-diazaisoindigo (AIID).[136] A copolymer of AIID and bithiophene, **P16** (Figure 15), possesses LUMO and HOMO energies of -3.64 eV and -5.67 eV, respectively, determined by the CV measurements. In BGBC OFET devices, unipolar p-type semiconductor performance with a maximum hole mobility of 7.28 $cm^2V^{-1}s^{-1}$ was achieved. On the other hand, in the TGBC devices, ambipolar charge transport with the maximum hole and electron mobilities of 2.33 and 0.78 $cm^2V^{-1}s^{-1}$, respectively, was achieved. The observation of electron transport behavior in the TGBC devices is due to the encapsulation effect of the dielectric and gate electrode layers above the polymer semiconductor, which could prevent the exposure of the semiconductor to the oxygen and moisture in the ambient environment. These results again demonstrated that a polymer with a LUMO energy above ca. -3.7 eV cannot achieve electron transport in ambient air.

Recently, McCulloch *at al*. reported a copolymer of AIID and selenophene (a weaker electron donor than thiophene), **P17**, which has a rather low LUMO energy of -4.0 eV.[137] This low LUMO energy facilitated electron injection and enabled electron transport. Electron mobilities as high as 0.5 $cm^2V^{-1}s^{-1}$ were obtained in TGBC OFETs. However, the HOMO energy is at -5.6 eV, which seems not low enough to suppress hole injection and transport and thus this polymer showed ambipolar charge transport performance although the electron transport is more favored. When the electron accepting benzothiadiazole was used as a comonomer unit, the resulting polymer **P18** exhibited both lower LUMO and HOMO energies at -4.1 eV and -5.8 eV, respectively. Unipolar n-type semiconductor performance was

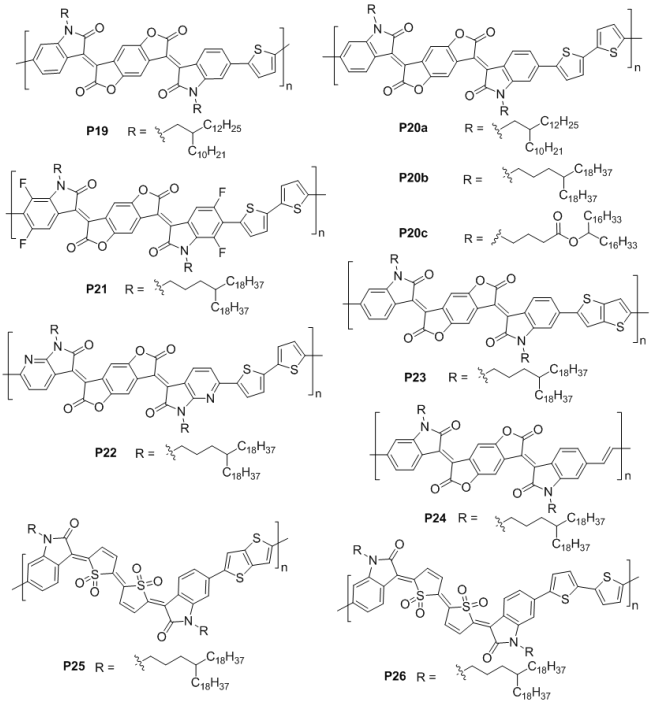

Figure 16. IBDF (**P19**-**P24**) and IDTO (**P25** and **P26**) based polymers.

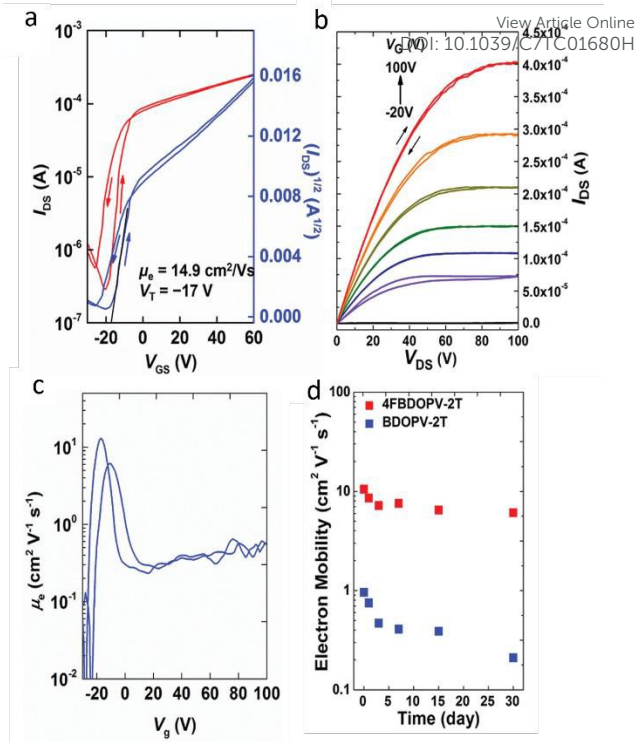

Figure 17. (a) and (b)Transfer and output characteristics of a TGBC OFET device based on **P21** annealed at 160 °C (L = 100 μm, W = 2000 μm) with an electron mobility of 14.9 $cm^2V^{-1}s^{-1}$ in the saturation regime in the V_{GS} range from -16 to -6 V. (c) Mobilities as a function of gate voltage. (D) Stability comparison of the **P21** (F4BDOPV-2T) and **P20b** (BDOPV-2T) based devices in ambient air (RH = 50%–60%). Reproduced with permission from ref. 23. Copyright 2016 John Wiley & Sons.

observed thanks to the reduced HOMO energy of this polymer. High electron mobilities of up to 1 $cm^2V^{-1}s^{-1}$ were achieved. DFT simulations showed that the AIID-selenophene or AIID-benzothiazole linkage is quite coplanar with a small dihedral angle of 5° due to the less sterically demanding nitrogen atoms at the 7-positions of AIID, in sharp contrast with the isoindigo analogues, which are much more twisted. This might explain the high carrier mobility achieved by **P17** and **P18**.

As aforementioned, IBDF is an excellent electron acceptor building block for small molecule n-type semiconductors with high electron mobility. The first IBDF containing polymer, **P19** (Figure 16) that consists of an IBDF and a thiophene in its repeat unit, was reported by Yan *et al*.[97] This polymer has a very low LUMO energy of -4.43 eV and also a relatively low HOMO energy of -5.79 eV. Unipolar n-type semiconductor performance was observed when the BGBC OFET devices were encapsulated with PMMA. The highest electron mobility is 5.4 × 10^{-3} $cm^2V^{-1}s^{-1}$. Interestingly the devices showed enhanced electron mobility up to 8.6 ×10^{-3} $cm^2V^{-1}s^{-1}$ and hole transport characteristics with mobility of up to 9.0 × 10^{-3} $cm^2V^{-1}s^{-1}$ when the semiconductor layer was exposed to ambient air. The enhanced electron mobility and appearance of hole transport behavior were explained by the doping of the semiconductor layer by oxygen and/or moisture in the air. The synthesis of an IBDF-bithiophene copolymer, **P20a**, was also reported in the same paper. However, this polymer was found insoluble in any solvents due to the strong intermolecular interactions. Later, Lei *et al*.[138] used a much large branched alkyl substituent containing 40 carbon atoms on the IBDF unit and the resulting polymer, **P20b**, became readily soluble. Unipolar n-type semiconductor performance was observed in both TGBC and BGBC OFETs. The highest electron mobility of 1.74 $cm^2V^{-1}s^{-1}$ was achieved for TGBC devices when the devices were fabricated in nitrogen. The BGBC devices showed electron mobilities of up to 0.13 $cm^2V^{-1}s^{-1}$, significantly lower than those of the TGBC devices. Similar to the phenomenon observed by Yan *et al*.,[97] the devices fabricated in ambient air showed ambipolar charge transport performance. He *et al*. reported another IBDF-BT copolymer, **P20c**, using the newly developed ester-type side chains, which is much easier to synthesize than the C40 side chain precursor in **P20b**.[139] In BGBC OFETs, quite balanced electron and hole mobilities of 0.35 $cm^2V^{-1}s^{-1}$ and 0.20 $cm^2V^{-1}s^{-1}$, respectively, were obtained. The electron mobilities are similar to those of its alkyl side chain counterpart, **P20b**, in the same BGBC device structure.

To improve the electron affinity of the IBDF core, Zheng *et al*. introduced four fluorine substituents.[23] The resulting polymer **P21** has lower LUMO and HOMO energies of -4.32 and -5.96 eV than those of **P20b** (-4.15 eV and -5.72 eV). The TGBC OFET devices with **P21** exhibited typical n-type semiconductor performance. A record high electron mobility of 14.9 $cm^2V^{-1}s^{-1}$ was achieved in the TGBC OFETs. The devices based on **P21** showed good air stability with only a 40% drop in mobility (from 10.6 $cm^2V^{-1}s^{-1}$ to 6.1 $cm^2V^{-1}s^{-1}$) after 30 days exposure to air, much better than the devices based on **P20b**, which showed a 78% drop in mobility (from 0.96 $cm^2V^{-1}s^{-1}$ to 0.21 $cm^2V^{-1}s^{-1}$).

However, kinked $I_D^{1/2}$-V_{GS} curves were observed for the **P21**-based OFETs with high mobilities (Figure 17). While a high mobility of 14.9 $cm^2V^{-1}s^{-1}$ was calculated in the low V_{GS} region, a much lower mobility of 1.24 $cm^2V^{-1}s^{-1}$ in the high V_{GS} region

was obtained using the MOSFET model (Eq. (1)). As mentioned earlier, the non-ideal kinked transfer curves might be accounted for by an abrupt drop in the gated contact resistance in the low V_{GS} region.[34,35] For **P21**, the authors ruled out the solvent to be the cause for the non-linear behaviour because similar trends were observed for the films deposited by using either *o*-dichlorobenzene (ODCB) or 1,1,2,2-tetrachloroethane (TCE).[23] Since a fluorine polymer Cytop, which is known to have few electron traps, was used as the dielectric, dielectric trapping is also unlikely to be the cause for the non-linear behaviour. The authors found that the percentage of devices with non-ideal transfer curves decreases with the spin coating speed used for fabricating the polymer films. At a low spin speed of 500 rpm, all devices showed non-ideal transfer characteristics, while at a high spin speed of 2500 rpm, only 19% of the devices showed non-ideal behavior (Figure 18). Through 2D-GIXD analysis, it was found that the crystallinity or the coherence length in the lamellar stacking of the polymer films increases with decreasing spin speed. Therefore, it seems that larger crystallite domains and better polymer stacking order have led to the non-ideal transfer characteristics of the OFETs. Previously, we used different routes to synthesize a series of p-type DDP-based polymers (PDQT with 2-octyldodecyl (C20) side chains), which contained varied amounts of structural defects (homo-coupled dimer units).[149] We also observed serious deviations of the transfer characteristics from the ideal MOSFET model for the OFETs with high mobilities. Since all the devices adopted the same device structure and were fabricated under the same conditions, the difference in the non-linear behavior between the high mobility and low mobility devices highly likely originated from their semiconductor layers with different polymers. Similar to the observation by Pei *et al*., we found that the non-ideal behavior became more apparent with increasing crystallinity (or chain packing order) of the polymer films. On the other hand, the number of structural defects, molecular weight, and thin film morphology do not have obvious correlations with the appearance of non-ideal transfer characteristics. The results of Pei's and ours might support the explanation by Takeya *et al*.[16] that the mobility at a lower V_{GS} represents the in-crystal charge carriers, while the reduction in mobility at a higher V_{GS} is contributed by the less ordered semiconductor/dielectric interface, where charge carrier trapping and scattering occur. If it is the case, the mobility extracted at the lower V_{GS} region of the transfer curve may reflect the highly ordered, crystalline domains of the semiconductor film, rather than being "overestimated". Hence, instead of saying that the contact resistance reduced abruptly in the low V_{GS} region, it might be more appropriate to say that the contact resistance increased abruptly at the high V_{GS} region, which might be due to the participation of the more disordered fractions of the polymer chains in the charge transport as the V_{GS} increases. The transfer characteristics severely deviated from the ideal MOSFET model may be problematic or not useful for the practical applications. However, the mobilites extracted in the low V_{GS} region using the ideal model may still be helpful for the understanding of the structure-charge transport relationship, particularly the potential/intrinsic charge

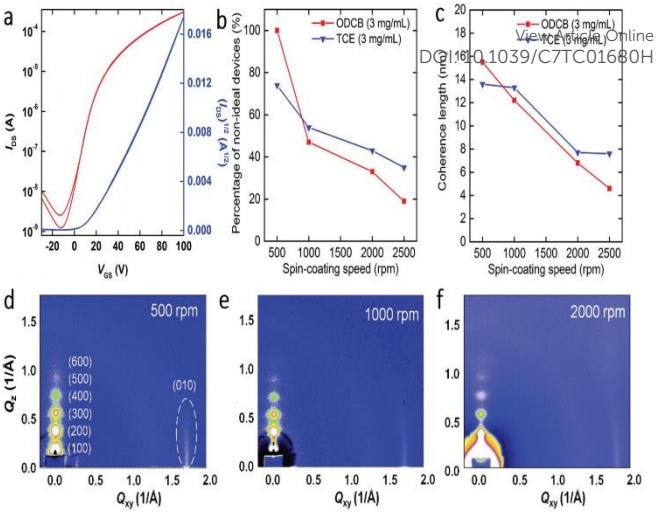

Figure 18. a) A near-ideal transfer characteristic observed for a **P21** based OFET devices (W = 2000 um, L = 100 um, V_{DS} = 100 V). b) The percentage of nonideal devices versus spin-coating speed using different solvents (over 20 devices were tested for each condition). c) Coherence length (L_c) variation versus spin-coating speed. The coherent lengths are calculated using the Scherrer equation based on the full width at half maximum of (200) diffraction peaks using GIXD data. 2D-GIXD patterns of **P21** films fabricated under different spin-coating speed (ODCB 3 mg mL^{-1}): d) 500 rpm, e) 1000 rpm, and f) 2000 rpm. Reproduced with permission from ref. 23. Copyright 2016 John Wiley & Sons.

transport property of the organic semiconductor, to design materials with enhanced charge transport performance. Further studies are needed to clarify the root cause for the "kinked" non-linear transfer characteristics and address this issue. For instance, the approach of decreasing crystallinity used by Pei *et al*. to eliminating the non-ideal transfer behaviour comes along with a significant reduction of carrier mobility. If the opposite approach of increasing crystallinity of the polymer films works, it would shed more light on the cause of the non-ideal transfer characteristics and would be more beneficial for improving the OFET performance.

Dai *et al*. introduced the more withdrawing pyridine ring to replace the benzene ring in BDOPV to form AzaBDOPV.[140] The copolymer of this new building block with bithiophene, **P22**, indeed showed lower LUMO/HOMO energies (-4.37 eV/-5.80 eV) than those of **P20b**. Unipolar n-type semiconductor performance with a highest mobility of 3.22 $cm^2V^{-1}s^{-1}$ was achieved. The improved mobility of **P22** was considered to be due to its lower LUMO and less conformational disorder compared to **P20b**.

When IBDF and thienothiophene were copolymerized, the resulting polymer **P23** showed ambipolar transport with well-balanced electron and hole mobilities of 1.37 $cm^2V^{-1}s^{-1}$ and 1.70 $cm^2V^{-1}s^{-1}$ in TGBC devices.[141] The LUMO and HOMO energies of this polymer are -3.93 eV and -5.60 eV, respectively. The higher HOMO energy of this polymer compared to **P20b** might explain its enhanced hole transport. However, the same polymer **P23** in a recent paper by Wang *et al*.[150] showed unipolar n-type semiconductor performance with a highest electron mobility of 0.65 $cm^2V^{-1}s^{-1}$ in BGBC OFETs. The environment for the device testing, high vacuum (3×10^{-4} mbar), might be contributed to the unipolar n-type performance of **P23** in this study, since moisture and/or oxygen may induce hole transport performance as mentioned earlier.[97] After 70 days exposure in

ambient air, the devices with **P23** maintained 50% of its electron mobility when measured in vacuum.[150]

Vinylene (-CH_2=CH_2-) is the second smallest π-conjugated electron donor after ethynylene (-C≡C-). The use of vinylene instead of bithiophene as the linkage is expected to increase the electron affinity of the resulting BDOPV-V copolymer, **P24**.[98] Very low LUMO and HOMO energies of -4.24 eV and -6.21 eV, respectively, were obtained for **P24** by the CV measurements. Unipolar electron transport performance was observed in TGBC OFETs. The highest electron mobility achieved is 1.1 $cm^2V^{-1}s^{-1}$. Devices showed good stability for 30 days in ambient conditions.

It is shown in the previous section that thiophene-*S*,*S*-dioxidized indophenine (IDTO) is a newly developed very strong electron acceptor. Deng *et al*. synthesized a copolymer of IDTO and thienothiophene, **PIDTOTT** (**P25**).[142] **P25** has a low LUMO energy of -3.98 eV, which would be sufficient for stable electron transport and a very low HOMO energy of -5.92 eV, which would build up a high energy barrier for hole injection. BGBC OFETs with spin coated **P25** showed characteristic unipolar n-type semiconductor performance with the highest electron mobility of 0.14 $cm^2V^{-1}s^{-1}$. Considering that the polymer films are rather disordered (amorphous), this mobility value is quite high. This is the first example that a thiophene-*S*,*S*-dioxide compound showed field effect performance. The devices performed similarly when characterized in nitrogen and ambient air. To improve the coplanarity of the polymer backbone and thus the crystallinity of the polymer films, bithiophene was used in place of thienothiophene.[143] The obtained polymer **PIDTOBT** (**P26**) indeed showed improved crystallinity. A lower LUMO energy of -4.09 eV and a higher HOMO energy of -5.78 eV than those of **P25** were observed, which indicates that the incorporation of bithiophene extended the main chain conjugation and led to a narrower band gap enabled by the more coplanar backbone structure. Slightly improved electron mobilities of up to 0.18 $cm^2V^{-1}s^{-1}$ were achieved for the **P26** based BGBC OFETs with Au contacts.

4. n-Doped organic semiconductors

Doping is a well-known process to tailor the electronic properties of a semiconductor by intentionally adding a small amount of foreign substance (impurity). Controlled doping is the foundation for the modern electronic industry where p- and n-type silicon semiconductors are made and used for the MOSFET based logic circuits.[151] The pioneering work on doping of the π-conjugated polymers by Heeger, MacDiarmid, and Shirakawa led to the discovery of highly electrically conductive polymers.[152–155] In the presence of an oxidant or acid, electron rich (p-type) polymer semiconductors such as polyacetylene, polyaniline, polypyrrole, and polythiophene can be p-doped to show high electrical conductivity of up to ~10^5 S cm^{-1}. On the other hand, electron deficient conjugated polymers can be n-doped with a reducing agent or base to increase electrical conductivity. In recent years, research into controlled doping of organic semiconductors with a small amount of dopants has intensified[156–159] since many doped organic semiconductors show much improved performances in OLEDs, OPV, OTFTs,[160,161] and thermoelectrics (TEs).[162] Molecular doping of an organic semiconductor may affect the electronic properties through three mechanisms, (A) charge transfer,[156,159] (B) charge carrier trapping,[163,164] and (C) charge carrier scattering,[163,164] depending on the relative frontier LUMO and HOMO energies between the organic semiconductor and the dopant compound (Figure 19). The n-doping is discussed below and the mechanisms apply to the p-doping similarly, but in an opposite manner. In scenario (A) shown in Figure 19, when the HOMO of the dopant is higher than the LUMO of the organic semiconductor, electrons readily transfer from the HOMO of the dopant to the LUMO of the organic semiconductor. As a result, the electrical conductivity increases accompanied by a redshift of the absorption spectrum of the doped organic semiconductor. In scenario (B), when the HOMO of the dopant is lower than the LUMO of organic semiconductor, but higher than the HOMO of the organic semiconductor, electron transfer from dopant to organic semiconductor is energetically prohibited; however, the mobile holes (injected from the source electrode in an OFET) may be trapped at the energetically more favoured HOMO of the dopant in comparison to the HOMO of the organic semiconductor. The HOMO energy difference (Δ*E*) between dopant and organic semiconductor is termed as trap depth or trap energy (E_T).[165,166] When E_T is < ca. 0.2 eV, the dopant forms shallow hole traps,[166–168] where holes can easily

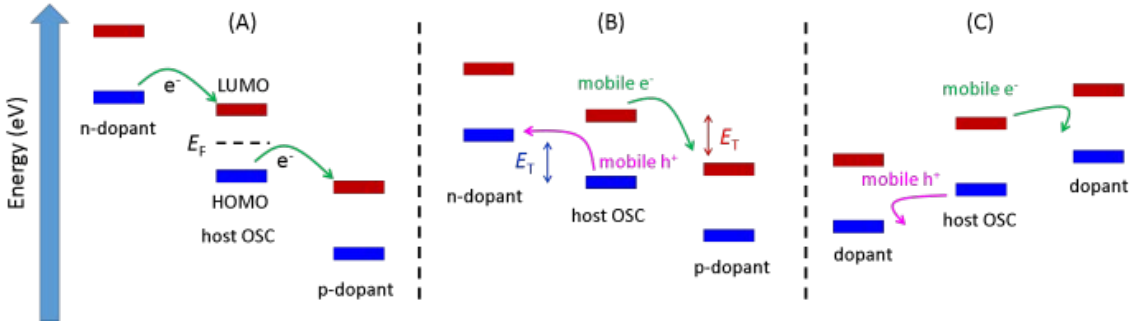

Figure 19. The energy level scheme of three doping mechanisms of an organic semiconductor (OSC) depending on the relative energy levels of the OSC and the dopant. (A) Electron transfer occurs when the HOMO energy of the dopant (or OSC) is higher than the LUMO energy of the OSC (or dopant), leading to the n-doping (or p-doping) or an OSC; (B) For n-doping, trapping of the injected holes occurs when the HOMO energy of the dopant is lower than the LUMO energy of the OSC, but higher than the HOMO energy of the OSC, leading to the suppression of the hole transport and enhancement of electron transport. Likewise, trapping of injected electrons occurs for p-doping. The HOMO or LUMO energy difference between the dopant and the OSC is termed as trap energy (E_T), where deep traps form when E_T > ca. 0.2 eV, while shallow traps form when E_T < ca. 0.2 eV. (C) Scattering of injected holes (or electrons) occurs when the HOMO (or LUMO) energy of the dopant is lower (or higher) than that of the OSC, which either decreases or enhances the hole (or electron) transport. The Fermi energy (E_F), which is positioned in the mid of the band gap of a pristine OSC, may increase or decrease with the addition of an electron rich or deficient dopant, which affects the charge injection and transport for the doped OSC in (B) and (C).

View Article Online
DOI: 10.1039/C7TC01680H

enter and can also exit with a small amount of energy. The shallow traps would slow down the hole transport or cause a decrease in hole mobility.[166] When E_T is > ca. 0.2 eV, the dopant forms deep hole traps, where holes can readily enter, but cannot exit or require a very high energy to exit. As a result, hole transport may be completely suppressed due to a dramatic decrease in the number of mobile holes. Some recent studies by the time-of-flight (TOF) measurement show that the presence of deep traps do not significantly reduce the mobility of charge carriers that are not trapped.[169,166,168] In scenario (C), when the HOMO of the organic semiconductor is higher than the HOMO of the dopant, but lower than the LUMO of the dopant, neither electron transfer from organic semiconductor to dopant nor hole trapping at the dopant sites would occur. In this case, the low-lying HOMO of the dopant would form an energy barrier and cause scattering of mobile holes. Similar to the shallow and deep traps, low and high scatters are divided by the HOMO energy difference between the dopant and the organic semiconductor (or so-called the height of the scatters) with a value smaller or greater than ca. 0.2 eV, respectively.[168] It was found that scatters influence the carrier mobility in a similar manner as shallow and deep traps, i.e., low scatters reduce the carrier mobility, while high scatters do not significantly affect the carrier mobility.[168] In the cases of (B) and (C), since no charge transfer occurs between the semiconductor and the dopant, there would be no changes in the UV-Vis-NIR absorption spectra and no increase in the electrical conductivity of the doped organic semiconductor if no charge carriers are injected into the doped organic semiconductor. Theoretical and experimental evidence shows that doping in scenarios (A) or (B) causes a shift of the Fermi energy of the semiconductor: a decrease for p-doping and a lift for n-doping.[159] A decreased Fermi energy or electron density of the semiconductor *via* p-doping would help fill the hole traps, while an increased Fermi energy (E_F) or electron density *via* n-doping would help fill electron traps. In addition, if the same electrode material is used, a raised or lowered E_F would also be beneficial for the electron or hole injection, respectively. Therefore, it is often observed that hole transport is enhanced for the p-doped organic semiconductors, while on the contrary electron transport is enhanced for n-doped organic semiconductors.

Compared to p-doping, n-doping is less studied because of the unavailability of stable n-dopants with high HOMO energy and organic semiconductors with very low LUMO energy. Nonetheless, n-doping of an organic semiconductor has a number of benefits for the OTFT application. First, the electron transport can be improved by the increased electron density through trap filling. Second, the hole transport can be suppressed, which can convert an ambipolar and even p-type organic semiconductor into an n-type semiconductor. Therefore, a great number of n-type organic semiconductors can potentially be obtained by n-doping known materials. In particular, a large number of D-A polymers have shown very high charge carrier mobilities. However, due to their rather high HOMO energy and low LUMO energy contributed mainly by the donor and acceptor units, respectively, many D-A polymers have shown ambipolar charge transport performance. Although

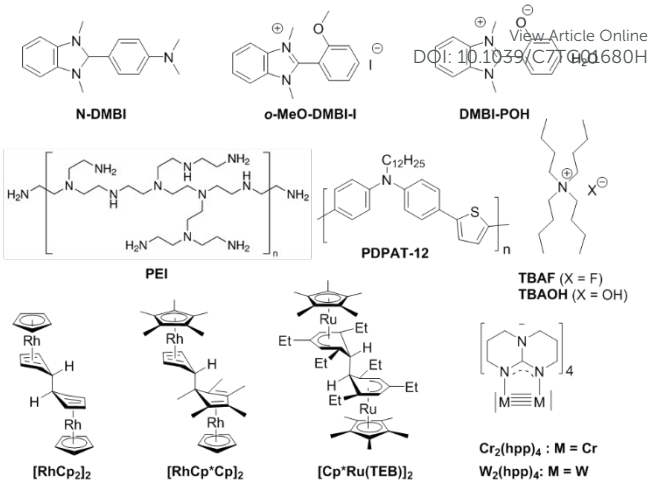

Figure 20. Structures of some organic and organometallic n-dopants.

the use of ambipolar polymers as single component semiconductors can greatly simplify the fabrication of CMOS-like complementary circuits, the devices suffer from high off currents and low I_{on}/I_{off} ratios, which results in high power consumption.[32] Therefore, converting ambipolar polymers into unipolar n-type or p-type polymers by doping to fabricate unipolar n- or p-channel OFETs with improved I_{on}/I_{off} ratios would open up new applications for ambipolar polymers. Third, n-doping (as well p-doping) can readily tune the threshold voltage (V_{th}) of an OTFT by controlling the filling of electron traps with a proper amount of dopant. A precise control of the threshold voltage of transistors is very important for fabricating integrated logic circuits.

In 2010 Bao *et al*. synthesized and used a stable (4-(1,3-dimethyl-2,3-dihydro-1*H*-benzoimidazol-2-yl)phenyl)dimethylamine (N-DMBI) (Figure 20) as an n-dopant to [6,6]-phenyl C_{61} butyric acid methyl ester ($PC_{61}BM$), which is an n-type semiconductor.[170] The electron mobility of the doped $PC_{61}BM$ markedly increased to 1.24×10^{-1} $cm^2V^{-1}s^{-1}$ from 1.68×10^{-2} $cm^2V^{-1}s^{-1}$ for the undoped $PC_{61}BM$ in OTFTs. It was also observed that V_{th} shifted negatively with increasing dopant concentration, indicating that mobile electron traps were filled by the DMBI molecules. The devices with the doped $PC_{61}BM$ demonstrated much improved air stability, which was attributed to the compensatory effect of the dopant on the O_2 electron traps. However, the off current increased significantly once the dopant concentration was greater than 2 mol%, resulting in a smaller current I_{on}/I_{off}. The UV-Vis-NIR spectrum of the N-DMBI doped $PC_{61}BM$ showed a new broad peak in the 800-1000 nm region, which suggested that strong doping, which might have involved charge transfer, indeed occurred. However, the n-doping effect of N-DMBI on $PC_{61}BM$ could not be interpreted by the energy levels shown in Figure 19 since the HOMO of N-DMBI is -4.67 eV, which is too low to allow electron transfer to the LUMO of $PC_{61}BM$ (-4.30 eV) as shown in scenario (A) and there should be no electron transfer in scenario (B). The authors initially proposed that the neutral radical formed at N-DMBI upon removal of hydrogen would allow the electron transfer.[170] Later on they further studied the doping mechanism

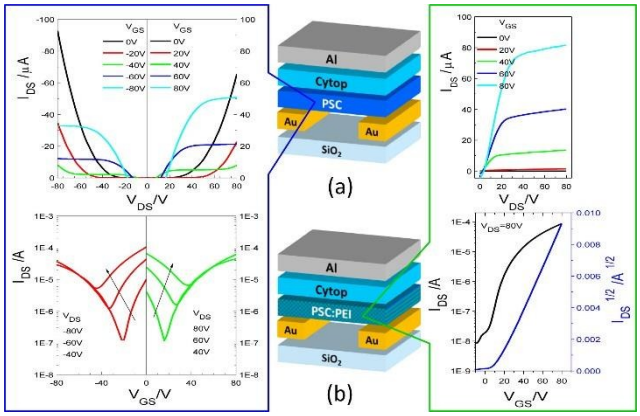

Figure 21. (a) TGBC OFET device structure with a pristine **P10** as the channel. The output (upper) and transfer (lower) curves on the left show ambipolar charge transport performance. (b) TGBC OTFT device structure similar to that in (a) except that the channel is a **P10**:PEI (2 wt%) blend film. The output (upper) and transfer (lower) curves on the right show n-channel electron-only transport performance. The **P10** and **P10**:PEI blend films were annealed at 150 °C. Dimensions of the devices: channel length L = 30 μm; channel width W = 1 mm. Reproduced with permission from ref. 129. Copyright 2015 American Chemical Society.

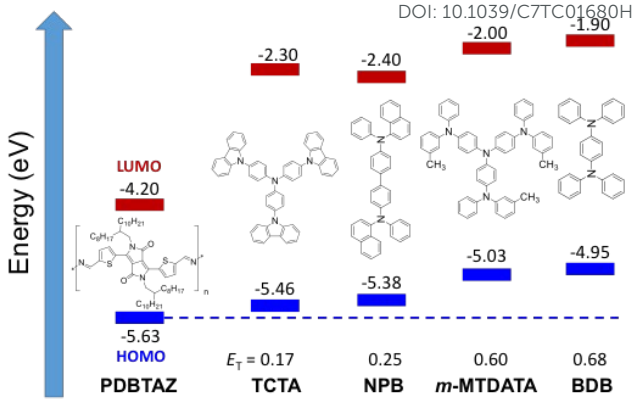

Figure 22. Chemical structures and HOMO energies of the host polymer semiconductor, **P10** (**PDBTAZ**), and four aromatic amine n-dopants. E_T is the trap energy of the dopant, which is the HOMO energy difference between the dopant and the polymer. Reproduced with permission from ref. 175. Copyright 2016 Elsevier.

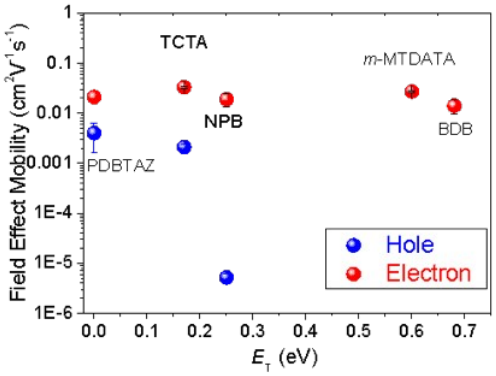

Figure 23. Relationship between the field effect mobilities of **P10** and its doped films with 2% dopant and E_T of the amine dopants. Reprinted with permission from ref. 175. Copyright 2016 by Elsevier.

of N-DMBI and several of its analogues and found that a reaction between the dopant and the host semiconductor occurred with either hydride or hydrogen atom transfer, forming host radical anions, which are accounted for the doping effect.[171] Interestingly, the typical p-type semiconductor, TIPS-pentacene, could be n-doped with 2-(2-methoxyphenyl)-1,3-dimethyl-2,3-dihydro-1H-benzoimidazole (*o*-MeO-DMBI), which is an analogue of N-DMBI.[172] The pristine TIPS-pentacene showed p-channel performance with hole mobility of 0.21 $cm^2V^{-1}s^{-1}$ in OFETs fabricated by solution shearing, while the TIPS-pentacene : *o*-MeO-DMBI (1:1) blend films exhibited electron transport dominant ambipolar transistor performance with a very high electron mobility of 6.8 $cm^2V^{-1}s^{-1}$ and a rather low hole mobility of 3.6 × 10^{-4} $cm^2V^{-1}s^{-1}$. Unlike the n-doping of fullerene derivatives, where OTFTs displayed reduced I_{on}/I_{off} at higher dopant concentrations, the OFETs of the TIPS-pentacene : *o*-MeO-DMBI blend showed very high I_{on}/I_{off} of ~10^5-10^6 (and low off current) even with an equivalent amount of dopant. The electrical conductivity of the organic semiconductors doped through electron transfer increases since the charge carrier density increases after doping, which generally results in an undesirable reduction in the I_{on}/I_{off} of OFETs. Therefore, this characteristic of the TIPS-pentacene : *o*-MeO-DMBI blend is particularly useful for OTFTs. The UV-Vis-NIR and photothermal deflection spectroscopies showed no evidence of formation of radical anions, suggesting that the doping of TIPS-pentacene by *o*-MeO-DMBI might have a different mechanism from that of the fullerene-DMBI systems. Very recently, the same group used this compound to n-dope a high mobility p-type donor–acceptor polymer poly(tetrathienacene-diketopyrrolopyrrole) (PTDPPTFT4) to induce a strong memory behavior in OFETs.[173] Hole trap density was found to increase with dopant concentration, showing strong suppression effect of this compound on hole transport. Again, no differences in the UV-Vis-NIR spectra between the pristine and the doped polymer films were observed. The authors proposed that (1) electron transfer may partially take place with surface defects, which allowed electron transport, and (2) holes may also transfer from the HOMO of the semiconductor to and be trapped at the dopant sites. *o*-MeO-DMBI has a HOMO energy of -4.67 eV, while TIPS-pentacene[174] and PTDPPTFT4[173] have HOMO/LUMO energies of -5.4 eV/-3.53 eV and -5.3 eV/-3.95 eV, respectively. Therefore, we believe the trapping mechanism illustrated in Figure 19B may apply to these systems, where *o*-MeO-DMBI would form deep hole traps (E_T > -0.2 eV).

Recently, our group used an amine-containing polymer, polyethylenimine (PEI), as an n-dopant for ambipolar (such as **P10** and **P14**) and p-type polymers.[129] Ultraviolet photoelectron spectroscopy (UPS) measurements showed that the Fermi energies of the doped polymers increased by 0.04-0.21 eV compared to the corresponding pristine polymers, indicating an increase in the electron density. Most of the doped polymers showed improved electron mobilities at a lower dopant concentration of < 2 wt%, which could be explained by the filling of mobile electron traps. On the other hand, all the polymers showed a disappearance of hole transport at a dopant concentration of 2 wt% or higher. For example, 2% PEI doped **P10** showed no hole transport performance, while the electron mobility significantly improved from ~0.4 $cm^2V^{-1}s^{-1}$ to as high as

View Article Online
DOI: 10.1039/C7TC01680H

0.88 $cm^2V^{-1}s^{-1}$ (Figure 21). This is a very convenient approach to obtaining n-type polymers by simply doping ambipolar and even p-type polymers with PEI. The suppression of hole transport was explained by the increased Fermi energy, which increased the hole injection barrier, and the strong interaction of the injected holes with the electron lone pairs of the nitrogen atoms in PEI, which retarded the movement of the holes. The UV-Vis-NIR spectra of the PEI-doped polymers displayed no noticeable changes compared to their corresponding pristine polymers, indicating that charge transfer between PEI and the polymer semiconductor is unlikely. Similar to the TIPS-pentacene : *o*-MeO-DMBI blend reported by Bao *et al*.,[172] the PEI-doped polymers showed very low off current (the electrical conductivity of the blend remains as low as that of the pristine polymers) and high I_{on}/I_{off}, which are very different from many other n-doped semiconductor systems that involve charge transfer and show decreased I_{on}/I_{off} due to their increased conductivity.

We also used several small molecule aromatic amine compounds (Figure 22), which are known organic semiconductors, as n-dopants for the ambipolar polymer **P10** in order to suppress hole transport and transform this polymer to unipolar n-type semiconductor.[175] The rationale is that if the HOMO energy of a dopant is sufficiently higher than that of the host semiconductor to create an E_T greater than ca. 0.2 eV, the holes in the channel may be trapped at the HOMO of the dopant (see Figure 19B). The common feature of these aromatic amine compounds is that they have higher HOMO energies than that of the host polymer semiconductor (-5.63 eV). E_T's of these amines against the polymer are in the range between 0.17 eV and 0.68 eV. It was found that when the E_T of an aromatic amine is $\geq$ 0.25 eV, a complete suppression of hole transport of the polymer and only electron transport behaviour were observed (Figure 23). As observed for the PEI-doped blends, the OTFTs with **P10** doped by these small amines showed low off current and high I_{on}/I_{off} of ~10^4-10^6. There were no changes in the UV-Vis-NIR spectra of the doped **P10**, which indicates that no electron transfer occurred between the dopant and the polymer and the doping mechanism of Figure 19B applies in this case.

To solve the issues of the high moisture sensitivity of PEI observed for the n-doped polymer blends, He *et al*. recently synthesized a novel aromatic amine based polymer, PDPAT-12 (Figure 20), as an n-dopant to **P20c**.[176] It was found that with addition of 10 wt% PDPAT-12, the doped **P20c** blend exhibited unipolar n-type semiconductor performance with electron mobilities of up to 0.42 $cm^2V^{-1}s^{-1}$, while the pristine **P20c** showed ambipolar charge transport behaviour with electron and hole mobilities of up to 0.35 $cm^2V^{-1}s^{-1}$ and 0.20 $cm^2V^{-1}s^{-1}$, respectively. Again the doped polymer films showed no changes in their UV-Vis-NIR spectra compared to the pristine polymer. The OFET devices with the PDPAT-12-doped P20c exhibited decreased off current of ~10^{-11} A and much increased I_{on}/I_{off} of ~10^6 compared to the pristine **P20c** based devices, which has much higher off current of ~10^{-8} to10^{-7} A and lower I_{on}/I_{off} of 10^2-10^3. The observed suppression of hole transport was interpreted by the hole trapping effects of PDPAT-12 as illustrated in Figure 19B, since this compound has a high HOMO energy of -5.27 eV that forms deep hole traps with an E_T of 0.45 eV relative to the HOMO energy of **P20c**, but a higher LUMO energy of -2.65 eV than that of **P20c** (-3.87 eV). The **P20c** film with 10 wt% PDPAT-12 has much smoother surface morphology forming a well-connected network compared to the pristine **P20c** film, which are ascribed to the improved electron mobility of the former. Since PDPAT-12 is hydrophobic, the BGBC devices with PDPAT-12-doped **P20c** films still maintained 50% of their initial mobilities after exposure to ambient air (RH = ~50%) for 28 days, whereas the devices PEI-doped **P20c** films lost transistor performance immediately after being exposed to ambient air. The devices with PDPAT-12-doped **P20c** showed even better air stability than the devices with the pristine **P20c** films, which retained only 13% of the initial mobilities. It was considered that the electron-rich aromatic amine PDPAT-12 might serve as an oxygen scavenger to oxygen diffused into the active layer, which led to the improved air stability of the PDPAT-12-doped **P20c**.

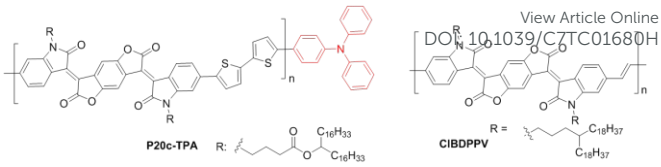

Figure 24. Structures of **P20c-TPA** and **CIBDPPV**.

Poor dispersion and phase segregation over time are the common problems for small molecule/polymer blends. To tackle these issues, Quinn *et al*. designed and synthesized a series of polymers (**P20c-TPA**) having varied amounts of triphenylamine (TPA) terminal groups (Figure 24).[177] It was expected that the aromatic amine groups would be able to function as n-dopant to self-dope the polymer chain, while the covalent bonding of the TPA end group to the polymer would improve the uniform and stable dispersion of the dopants and solve the phase separation issue mentioned above. The chosen pristine polymer **P20c** is an ambipolar semiconductor with quite balanced electron and hole mobilities.[139] The estimated trap energy E_T of TPA and the polymer using computer simulation is 0.46 eV, which is sufficient for trapping holes (Figure 19B). Therefore, the hole transport is expected to be suppressed. Indeed, as the amount of the TPA groups increased, the hole mobility decreases, while the electron mobility remains similar. An electron and hole mobility ratio (μ_e/μ_h) of 25.6 was achieved, which is much higher than that of the pristine polymer without TPA end-capping (μ_e/μ_h = 0.96), *i.e*., the polymers were transformed from ambipolar to n-type dominant by the simple TPA end-capping. These self-n-doped polymers showed much better stability in terms of the μ_e/μ_h ratio when thermally annealed at temperatures up to 200 °C compared to the small amine/polymer blends,[175] which showed a recovery of hole transport at much lower annealing temperatures of 80–100°C caused by phase separation.

Noh *et al.* n-doped $PC_{61}BM$ by blending a small amount of cesium fluoride (CsF).[178] The Fermi energy and electron concentration of the doped $PC_{61}BM$ significantly increased with

View Article Online
DOI: 10.1039/C7TC01680H

increasing amount of CsF. For example, at a CsF concentration of 1 wt%, the Fermi energy was lifted by 0.32 eV, while the electron concentration was increased by six orders of magnitude. As a result, the minority electron carriers in the pristine $PC_{61}BM$ became the majority carriers in the doped $PC_{61}BM$ and electron transport was enhanced. With the pristine $PC_{61}BM$, the OFET devices showed rather balanced electron and hole mobilities of 0.067 $cm^2V^{-1}s^{-1}$ and 0.030 $cm^2V^{-1}s^{-1}$, respectively. With increasing amount of CsF, the hole mobility decreased significantly, while the electron mobility increased. At a dopant concentration of 1 wt%, the electron transport (with mobility of 0.13 $cm^2V^{-1}s^{-1}$) becomes dominant over the hole transport (with mobility of merely 5.9 x 10^{-5} $cm^2V^{-1}s^{-1}$). CsF was also used as an n-dopant for P(NDI2OD-T2) (**P1a**).[179] Slightly improved electron mobility and reduced off current were obtained when the dopant concentration was controlled below 1 wt%. Very recently, Kim *et al*. found that tetrabutylammonium fluoride (TBAF) and tetrabutylammonium hydroxide (TBAOH) (Figure 20), which contain Lewis base anions, F– and OH–, could effectively n-dope **P1a**.[180] The UPS data revealed that the E_F shifted upward by 0.3 and 0.2 eV from that of the pristine **P1a** after adding 5% of TBAF and TBAOH, respectively, indicating n-doping of the polymer. In addition, dramatic changes around 500 nm in the UV-Vis absorption spectra were observed for the blend films, further supporting the occurrence of charge transfer upon n-doping. Compared with the pristine **P1a**, which showed n-type dominant performance with average electron and hole mobilities of 0.31 $cm^2V^{-1}s^{-1}$ and 0.004 $cm^2V^{-1}s^{-1}$, respectively, the doped **P1a** with 0.5% TBAF exhibited n-type-only unipolar performance with enhanced electron mobility of 0.67 $cm^2V^{-1}s^{-1}$. The TBAOH doped polymer films also showed improved electron mobility to 0.41 $cm^2V^{-1}s^{-1}$ and a substantial suppression of hole transport (μ_h = 0.0001 $cm^2V^{-1}s^{-1}$). The improved electron mobility and suppression of hole transport were accounted for by the reduced contact resistance due to the raised Fermi energy that reduced/increased the electron/hole injection barrier. Katz *et al.*[181] n-doped an IBDF-vinylene polymer **ClBDPPV** (Figure 24) with TBAF and used it as an n-type conductor for thermoelectric devices. **ClBDPPV** has LUMO and HOMO energies of -4.3 eV and -5.9 eV, respectively. In TGBC OFETs, this polymer showed electron mobilities of up to 0.104 $cm^2V^{-1}s^{-1}$ with an I_{on}/I_{off} of 10^4). With 25 wt% TBAF doping, the blend polymer film showed appearance of absorption in the long wavelength regions from 1000 nm to 1600 nm and from1600 nm to >2000 nm, which are due to the polaronic absorptions. The UPS measurement of the **ClBDPPV** film doped with 25 wt% of TBAF showed an upward shift of E_F by 0.35 eV compared to the pristine polymer. Furthermore, the electron spin resonance (ESR) spectra of the doped polymer clearly showed the paramagnetic signals of the anion radicals. These experimental data strongly supported the occurrence of electron transfer from F^- anions to the polymer. **ClBDPPV** doped with 25 wt% TBAF exhibited a very high electron conductivity of 0.62 S cm^{-1} and a thermoelectric power factor of 0.63 μW m^{-1} K^{-2}. After one week storage in ambient air, the doped **ClBDPPV** films still showed electron conductivity of over 0.1 S cm^{-1}. N-type organic semiconductors with such high conductivity and air stability are very rare.

Leo *et al*. found that dimetal compounds, tetrakis(1,3,4,6,7,8-hexahydro-2H-pyrimido[1,2-a]pyrimidinato)dichromium ($Cr_2(hpp)_4$) and -ditungsten ($W_2(hpp)_4$) (Figure 20), are much stronger n-dopants to C_{60} than to 3,6-bis(dimethylamino)acridine (AOB) and 2-(1,3-dimethyl-1*H*-benzoimidazol-3-ium-2-yl)phenolatehydrate (DMBI-POH).[182181182181180181180179178177176175174] These dimetal compounds have very high HOMO energies (e.g., -2.4 eV for $W_2(hpp)_4$),[183] which allows very efficient electron transfer from these dopants to the semiconductor. Dramatic increases in conductivity were observed at a very low dopant to semiconductor molar ratio (MR) of down to 10^{-5}. The $Cr_2(hpp)_4$ and $W_2(hpp)_4$ doped C_{60} also showed much higher electron mobilities. The same group successfully demonstrated the first realization of inversion OFETs by n-doping a very thin layer of pentacene with $W_2(hpp)_4$ at the interface to the gate dielectric.[184] These inversion OTFTs can overcome the drawback of low I_{on}/I_{off} for the common OFETs with doped semiconductors and can also precisely control the threshold voltage. However, due to the highly positioned HOMO level of $W_2(hpp)_4$,this compound is very unstable in air and the doped semiconductor degrades rapidly once exposed to air.[185] Very recently, Leo *et al*. found that if the LUMO energy of the host semiconductor is sufficiently low (e.g., <-3.6 eV), it can prevent the further charge transfer of the dopant-semiconductor charge transfer complex to the oxygen-water complexes,[186] which are considered the cause for the ambient degradation of OFETs.[187] Therefore, for the host semiconductors with LUMO energies higher than -3.6 eV, e.g., pentacene (-2.7 eV) and ZnPc (-3.4 eV), the $W_2(hpp)_4$ doped materials are unstable in air, while *N*,*N*-bis(fluorene-2-yl)-naphthalenetetracarboxylic diimide (bis-HFl-NTCDI) (E_{LUMO} = -3.6 eV) could form an air stable complex with $W_2(hpp)_4$.

Another type of stable n-dopants are dimers of metalocenes such as rhodocene ($[RhCp_2]_2$) and ruthenium(pentamethylcyclopentdienyl) (1,3,5-triethylbenzene) ($[Cp^*Ru(TEB)]_2$) (Figure 20).[188,189] These dimers can readily react with a number of n-type and p-type small molecule and polymer semiconductors to form monomeric metallocene cations and semiconductor radical anions, which were substantiated by the ^1H NMR and UV-vis-NIR spectroscopies. The UPS and inverse photoemission spectroscopy (IPES) data showed that the Fermi energies of the doped semiconductor films increased by 0.2-1.6 eV.[188] Conductivity as well as electron mobility of the $[RhCp^*Cp]_2$-doped **P1a** were also found to increase significantly.[190]

5. Conclusions

In the past five years or so, numerous novel n-type small molecule and polymer semiconductors have been reported. One approach frequently used has been on the optimization and modification of existing popular electron acceptor building blocks as such NDI, PDI, DPP, etc. Much improved electron mobilities of up to 8.6 $cm^2V^{-1}s^{-1}$ (**S3a**) for small molecule n-type

semiconductors and 6.5 $cm^2V^{-1}s^{-1}$ (**P1e**) for n-type polymer semiconductors were achieved.

Much effort has also been made to develop new electron acceptor building blocks. Several classes of materials with these new building blocks, such as small molecules based on azulene derivatives, dicyanomethylene-terminated quinoidal oligothiophenes, and isoindigo derivatives, and polymers based on DPP and isoindigo-derived building blocks, have shown very promising electron transport properties. For example, IBDF small molecules showed extremely high electron mobility of up to 12.6 $cm^2V^{-1}s^{-1}$ (**S26d**) in signal crystals, while solution processed IBDF polymers also demonstrated the highest electron mobility of 14.9 $cm^2V^{-1}s^{-1}$ (**P21**) reported so far. It should be mentioned that some of the high electron mobilities (such as the highest mobility reported for **P21**) were extracted from the low V_{GS} region of "kinked" non-ideal transfer curves, while the mobilities extracted from the high V_{GS} of the same transfer curves are lower by more than one order of magnitude. Recently, there have been some debates on if the high mobility values in the low V_{GS} are overestimated. Based on some studies including ours, we believe that at least in some cases the mobility extracted in the low V_{GS} might reflect the highly ordered crystalline domains of the organic semiconductors, rather than being overestimated. These mobilities may still be helpful for gaining insight into the structure-charge transport relationship, which is critical for the design of new organic semiconductors or the optimization of processing conditions for the known materials to further enhance charge transport performance in OFETs.

To address the undesirable hole transport characteristics and maintain or enhance the electron transport performance of ambipolar semiconductors, two approaches have been adopted. The first one is to modify the source contact to raise the Fermi energy of the conductor in order to block the hole injection as well as to facilitate the electron transport. Several ambipolar polymers have been successfully converted into unipolar n-type polymers. The second approach is to simply blend a small amount of n-dopant to n-unipolarize ambipolar organic semiconductors or even p-type semiconductors. Amine containing compounds such as *o*-MeO-DMBI, aromatic amines, and PEI were found very effective to suppress hole transport and promote electron transport without increasing the off current of the OFETs. It is believed that the Fermi energy of the organic semiconductors is raised by the electron rich n-dopant to effectively fill electron traps thus enhancing the electron transport. On the other hand, the electron lone pairs of the nitrogen atoms in these n-dopants would probably act as trapping sites to suppress hole transport. It was also found that the charge carrier trapping of a dopant can be readily applied to convert ambipolar or p-type polymers into unipolar n-type polymers. When the trap energy, the difference between the HOMO energies of the n-dopant and the matrix semiconductor, is greater than ca. 0.2 eV, complete hole transport suppression is observed. An n-dopant with such as a high ET would act as deep traps for the injected holes. N-doping seems a very promising strategy to utilize high mobility ambipolar organic semiconductors for unipolar n-channel OFETs.

In summary, impressive progresses have been made in the development of n-type organic semiconductors with electron mobilities approaching those of the best hole mobilities achieved by p-type organic semiconductors. However, the number of available suitable acceptor building blocks for n-type organic semiconductors is still much limited compared to electron donating building blocks. Furthermore, there are still very few truly unipolar pristine n-type polymers since many electron transport polymers also exhibit hole transport characteristics. More efforts are needed to explore new acceptor building blocks for unipolar n-type polymers. The choice of a comonomer building block for the acceptor is also very important. Excessively strong electron donating ability or too large the size of the donor comonomer would result in the appearance of hole transport characteristics.

Air stability is very important for device fabrication and long-term device operation. The stable n-channel OEFTs based on small molecules reported so far have been mostly the ones using single crystals, which prevented diffusion of oxygen and moisture into to active charge transport layer. On the other hand, almost all the stable n-channel OFETs based on polymers have been achieved in TGBC device architecture, where the semiconductor later was protected by the top dielectric and gape electrode layers from exposure to ambient air. Further attention should be paid to study and further improve the air stability of the n-type semiconductors.

It should be noted that n-type organic semiconductors (and their doped form) are also Indispensable materials for several other types of organic electronics such as organic photovoltaics,[82,83,107,191–194] thermoelectrics,[181,195,196] and batteries.[197,198] New materials and knowledge gained through the development of n-type organic semiconductors will be very helpful for the advancement of those neighboring applications.

Acknowledgements

YL thanks the Natural Sciences and Engineering Research Council (NSERC) of Canada for financial support of this work (Discovery Grants # RGPIN-2016-04366).

References

1 G. Horowitz, *Adv. Mater.*, 1998, **10**, 365–377.
2 C. D. Dimitrakopoulos and P. R. L. Malenfant, *Adv. Mater.*, 2002, **14**, 99–117.
3 H. Sirringhaus, *Adv. Mater.*, 2014, **26**, 1319–1335.
4 K. Fukuda, Y. Takeda, Y. Yoshimura, R. Shiwaku, L. T. Tran, T. Sekine, M. Mizukami, D. Kumaki and S. Tokito, *Nat. Commun.*, 2014, **5**, 4147.
5 M. Kaltenbrunner, T. Sekitani, J. Reeder, T. Yokota, K. Kuribara, T. Tokuhara, M. Drack, R. Schwödiauer, I. Graz, S. Bauer-Gogonea, S. Bauer and T. Someya, *Nature*, 2013, **499**, 458–463.
6 T. Sekitani, U. Zschieschang, H. Klauk and T. Someya, *Nat. Mater.*, 2010, **9**, 1015–1022.
7 K. Myny, S. Steudel, S. Smout, P. Vicca, F. Furthner, B. van der Putten, A. K. Tripathi, G. H. Gelinck, J. Genoe and W. Dehaene, *Org. Electron.*, 2010, **11**, 1176–1179.

8 M. E. Roberts, S. C. B. Mannsfeld, N. Queralto, C. Reese, J. Locklin, W. Knoll and Z. Bao, *Proc. Natl. Acad. Sci.*, 2008, **105**, 12134–12139.
9 X. Guo, A. Facchetti and T. J. Marks, *Chem. Rev.*, 2014, **114**, 8943–9021.
10 J. Mei, Y. Diao, A. L. Appleton, L. Fang and Z. Bao, *J. Am. Chem. Soc.*, 2013, **135**, 6724–6746.
11 Y. Li, P. Sonar, L. Murphy and W. Hong, *Energy Environ. Sci.*, 2013, **6**, 1684.
12 Y. He, W. Hong and Y. Li, *J Mater Chem C*, 2014, **2**, 8651–8661.
13 C. B. Nielsen, M. Turbiez and I. McCulloch, *Adv. Mater.*, 2013, **25**, 1859–1880.
14 S. Holliday, J. E. Donaghey and I. McCulloch, *Chem. Mater.*, 2014, **26**, 647–663.
15 B. S. Ong, Y. Wu, Y. Li, P. Liu and H. Pan, *Chem. - Eur. J.*, 2008, **14**, 4766–4778.
16 J. Takeya, M. Yamagishi, Y. Tominari, R. Hirahara, Y. Nakazawa, T. Nishikawa, T. Kawase, T. Shimoda and S. Ogawa, *Appl. Phys. Lett.*, 2007, **90**, 102120.
17 J. Liu, H. Zhang, H. Dong, L. Meng, L. Jiang, L. Jiang, Y. Wang, J. Yu, Y. Sun, W. Hu and A. J. Heeger, *Nat. Commun.*, 2015, **6**, 10032.
18 Y. Yuan, G. Giri, A. L. Ayzner, A. P. Zoombelt, S. C. B. Mannsfeld, J. Chen, D. Nordlund, M. F. Toney, J. Huang and Z. Bao, *Nat. Commun.*, 2014, **5**, 3005.
19 C. Luo, A. K. K. Kyaw, L. A. Perez, S. Patel, M. Wang, B. Grimm, G. C. Bazan, E. J. Kramer and A. J. Heeger, *Nano Lett.*, 2014, **14**, 2764–2771.
20 J. Li, Y. Zhao, H. S. Tan, Y. Guo, C.-A. Di, G. Yu, Y. Liu, M. Lin, S. H. Lim, Y. Zhou, H. Su and B. S. Ong, *Sci. Rep.*, 2012, **2**, 754.
21 I. Kang, H.-J. Yun, D. S. Chung, S.-K. Kwon and Y.-H. Kim, *J. Am. Chem. Soc.*, 2013, **135**, 14896–14899.
22 G. Kim, S.-J. Kang, G. K. Dutta, Y.-K. Han, T. J. Shin, Y.-Y. Noh and C. Yang, *J. Am. Chem. Soc.*, 2014, **136**, 9477–9483.
23 Y.-Q. Zheng, T. Lei, J.-H. Dou, X. Xia, J.-Y. Wang, C.-J. Liu and J. Pei, *Adv. Mater.*, 2016, **28**, 7213–7219.
24 C. R. Newman, C. D. Frisbie, D. A. da Silva Filho, J.-L. Brédas, P. C. Ewbank and K. R. Mann, *Chem. Mater.*, 2004, **16**, 4436–4451.
25 X. Gao and Y. Hu, *J. Mater. Chem. C*, 2014, **2**, 3099–3117.
26 X. Zhao and X. Zhan, *Chem. Soc. Rev.*, 2011, **40**, 3728–3743.
27 Y. Zhao, Y. Guo and Y. Liu, *Adv. Mater.*, 2013, **25**, 5372–5391.
28 J. E. Anthony, A. Facchetti, M. Heeney, S. R. Marder and X. Zhan, *Adv. Mater.*, 2010, **22**, 3876–3892.
29 J. Zaumseil and H. Sirringhaus, *Chem. Rev.*, 2007, **107**, 1296–1323.
30 D. M. de Leeuw, M. M. J. Simenon, A. R. Brown and R. E. F. Einerhand, *Synth. Met.*, 1997, **87**, 53–59.
31 H. Yan, Z. Chen, Y. Zheng, C. Newman, J. R. Quinn, F. Dötz, M. Kastler and A. Facchetti, *Nature*, 2009, **457**, 679–686.
32 M. Bronner, A. Opitz and W. Brütting, *Phys. Status Solidi A*, 2008, **205**, 549–563.
33 H. Sirringhaus, *Adv. Mater.*, 2005, **17**, 2411–2425.
34 T. Uemura, C. Rolin, T.-H. Ke, P. Fesenko, J. Genoe, P. Heremans and J. Takeya, *Adv. Mater.*, 2016, **28**, 151–155.
35 E. G. Bittle, J. I. Basham, T. N. Jackson, O. D. Jurchescu and D. J. Gundlach, *Nat. Commun.*, 2016, **7**, 10908.
36 I. McCulloch, A. Salleo and M. Chabinyc, *Science*, 2016, **352**, 1521–1522.
37 G. Horowitz, R. Hajlaoui, H. Bouchriha, R. Bourguiga and M. Hajlaoui, *Adv. Mater.*, 1998, **10**, 923–927.
38 D. Braga and G. Horowitz, *Adv. Mater.*, 2009, **21**, 1473–1486.
39 B. A. Jones, A. Facchetti, M. R. Wasielewski and T. J. Marks, *J. Am. Chem. Soc.*, 2007, **129**, 15259–15278.
40 H. Usta, A. Facchetti and T. J. Marks, *Acc. Chem. Res.*, 2011, **44**, 501–510.
41 X. Zhan, A. Facchetti, S. Barlow, T. J. Marks, M. A. Ratner, M. R. Wasielewski and S. R. Marder, *Adv. Mater.*, 2011, **23**, 268–284.
42 D. Shukla, S. F. Nelson, D. C. Freeman, M. Rajeswaran, W. G. Ahearn, D. M. Meyer and J. T. Carey, *Chem. Mater.*, 2008, **20**, 7486–7491.
43 H. E. Katz, A. J. Lovinger, J. Johnson, C. Kloc, T. Siegrist, W. Li, Y.-Y. Lin and A. Dodabalapur, *Nature*, 2000, **404**, 478–481.
44 B. J. Jung, K. Lee, J. Sun, A. G. Andreou and H. E. Katz, *Adv. Funct. Mater.*, 2010, **20**, 2930–2944.
45 C.-C. Kao, P. Lin, C.-C. Lee, Y.-K. Wang, J.-C. Ho and Y.-Y. Shen, *Appl. Phys. Lett.*, 2007, **90**, 212101.
46 C.-C. Kao, P. Lin, Y.-Y. Shen, J.-Y. Yan, J.-C. Ho, C.-C. Lee and L.-H. Chan, *Synth. Met.*, 2008, **158**, 299–305.
47 D. Zhang, L. Zhao, Y. Zhu, A. Li, C. He, H. Yu, Y. He, C. Yan, O. Goto and H. Meng, *ACS Appl. Mater. Interfaces*, 2016, **8**, 18277–18283.
48 Z. Yuan, Y. Ma, T. Geßner, M. Li, L. Chen, M. Eustachi, R. T. Weitz, C. Li and K. Müllen, *Org. Lett.*, 2016, **18**, 456–459.
49 W.-Y. Lee, J. H. Oh, S.-L. Suraru, W.-C. Chen, F. Würthner and Z. Bao, *Adv. Funct. Mater.*, 2011, **21**, 4173–4181.
50 T. He, M. Stolte and F. Würthner, *Adv. Mater.*, 2013, **25**, 6951–6955.
51 X. Chen, Y. Guo, L. Tan, G. Yang, Y. Li, G. Zhang, Z. Liu, W. Xu and D. Zhang, *J Mater Chem C*, 2013, **1**, 1087–1092.
52 X. Gao, C. Di, Y. Hu, X. Yang, H. Fan, F. Zhang, Y. Liu, H. Li and D. Zhu, *J. Am. Chem. Soc.*, 2010, **132**, 3697–3699.
53 F. Zhang, Y. Hu, T. Schuettfort, C. Di, X. Gao, C. R. McNeill, L. Thomsen, S. C. B. Mannsfeld, W. Yuan, H. Sirringhaus and D. Zhu, *J. Am. Chem. Soc.*, 2013, **135**, 2338–2349.
54 Y. Hu, Y. Qin, X. Gao, F. Zhang, C. Di, Z. Zhao, H. Li and D. Zhu, *Org. Lett.*, 2012, **14**, 292–295.
55 Y. Hu, Z. Wang, X. Zhang, X. Yang, C. Ge, L. Fu and X. Gao, *Org. Lett.*, 2017, **19**, 468–471.
56 Y. Fukutomi, M. Nakano, J.-Y. Hu, I. Osaka and K. Takimiya, *J. Am. Chem. Soc.*, 2013, **135**, 11445–11448.
57 M. Nakano, I. Osaka, D. Hashizume and K. Takimiya, *Chem. Mater.*, 2015, **27**, 6418–6425.
58 W. Fan, C. Liu, Y. Li and Z. Wang, *Chem. Commun.*, 2016, **53**, 188–191.
59 X. Cui, C. Xiao, L. Zhang, Y. Li and Z. Wang, *Chem. Commun.*, 2016, **52**, 13209–13212.
60 A. Lv, S. R. Puniredd, J. Zhang, Z. Li, H. Zhu, W. Jiang, H. Dong, Y. He, L. Jiang, Y. Li, W. Pisula, Q. Meng, W. Hu and Z. Wang, *Adv. Mater.*, 2012, **24**, 2626–2630.
61 L. M. Kozycz, C. Guo, J. G. Manion, A. J. Tilley, A. J. Lough, Y. Li and D. S. Seferos, *J. Mater. Chem. C*, 2015, **3**, 11505–11515.
62 A. J. Tilley, C. Guo, M. B. Miltenburg, T. B. Schon, H. Yan, Y. Li and D. S. Seferos, *Adv. Funct. Mater.*, 2015, **25**, 3321–3329.
63 Y. Wang, H. Guo, S. Ling, I. Arrechea-Marcos, Y. Wang, J. T. López Navarrete, R. P. Ortiz and X. Guo, *Angew. Chem. Int. Ed.*, , DOI:10.1002/anie.201702225.
64 C. Di, J. Li, G. Yu, Y. Xiao, Y. Guo, Y. Liu, X. Qian and D. Zhu, *Org. Lett.*, 2008, **10**, 3025–3028.
65 G. Gruntz, H. Lee, L. Hirsch, F. Castet, T. Toupance, A. L. Briseno and Y. Nicolas, *Adv. Electron. Mater.*, 2015, **1**, 1500072.
66 C. Wang, J. Zhang, G. Long, N. Aratani, H. Yamada, Y. Zhao and Q. Zhang, *Angew. Chem. Int. Ed.*, 2015, **54**, 6292–6296.

67 Y. Yamaguchi, Y. Maruya, H. Katagiri, K. Nakayama and Y. Ohba, *Org. Lett.*, 2012, **14**, 2316–2319.
68 Y. Yamaguchi, K. Ogawa, K. Nakayama, Y. Ohba and H. Katagiri, *J. Am. Chem. Soc.*, 2013, **135**, 19095–19098.
69 Y. Yamaguchi, M. Takubo, K. Ogawa, K. Nakayama, T. Koganezawa and H. Katagiri, *J. Am. Chem. Soc.*, 2016, **138**, 11335–11343.
70 H. Xin, C. Ge, X. Yang, H. Gao, X. Yang and X. Gao, *Chem Sci*, 2016, **7**, 6701–6705.
71 H. Xin, C. Ge, L. Fu, X. Yang and X. Gao, *Chin. J. Org. Chem.*, 2017, **37**, 711.
72 Q. Wu, R. Li, W. Hong, H. Li, X. Gao and D. Zhu, *Chem. Mater.*, 2011, **23**, 3138–3140.
73 C. Zhang, Y. Zang, E. Gann, C. R. McNeill, X. Zhu, C. Di and D. Zhu, *J. Am. Chem. Soc.*, 2014, **136**, 16176–16184.
74 C. Zhang, Y. Zang, F. Zhang, Y. Diao, C. R. McNeill, C. Di, X. Zhu and D. Zhu, *Adv. Mater.*, 2016, **28**, 8456–8462.
75 Y. Xiong, J. Tao, R. Wang, X. Qiao, X. Yang, D. Wang, H. Wu and H. Li, *Adv. Mater.*, 2016, **28**, 5949–5953.
76 S. Xu, N. Ai, J. Zheng, N. Zhao, Z. Lan, L. Wen, X. Wang, J. Pei and X. Wan, *RSC Adv.*, 2015, **5**, 8340–8344.
77 J.-H. Dou, Y.-Q. Zheng, Z.-F. Yao, Z.-A. Yu, T. Lei, X. Shen, X.-Y. Luo, J. Sun, S.-D. Zhang, Y.-F. Ding, G. Han, Y. Yi, J.-Y. Wang and J. Pei, *J. Am. Chem. Soc.*, 2015, **137**, 15947–15956.
78 J.-H. Dou, Y.-Q. Zheng, Z.-F. Yao, T. Lei, X. Shen, X.-Y. Luo, Z.-A. Yu, S.-D. Zhang, G. Han, Z. Wang, Y. Yi, J.-Y. Wang and J. Pei, *Adv. Mater.*, 2015, **27**, 8051–8055.
79 H. Hwang, D. Khim, J.-M. Yun, E. Jung, S.-Y. Jang, Y. H. Jang, Y.-Y. Noh and D.-Y. Kim, *Adv. Funct. Mater.*, 2015, **25**, 1146–1156.
80 Y. Deng, B. Sun, J. Quinn, Y. He, J. Ellard, C. Guo and Y. Li, *RSC Adv.*, 2016, **6**, 45410–45418.
81 Y. Hu, Z. Wang, X. Yang, Z. Zhao, W. Han, W. Yuan, H. Li, X. Gao and D. Zhu, *Tetrahedron Lett.*, 2013, **54**, 2271–2273.
82 F. Fernández-Lázaro, N. Zink-Lorre and Á. Sastre-Santos, *J Mater Chem A*, 2016, **4**, 9336–9346.
83 Z. Liu, Y. Wu, Q. Zhang and X. Gao, *J Mater Chem A*, 2016, **4**, 17604–17622.
84 W. Chen, J. Zhang, G. Long, Y. Liu and Q. Zhang, *J Mater Chem C*, 2015, **3**, 8219–8224.
85 X. Guo, R. P. Ortiz, Y. Zheng, Y. Hu, Y.-Y. Noh, K.-J. Baeg, A. Facchetti and T. J. Marks, *J. Am. Chem. Soc.*, 2011, **133**, 1405–1418.
86 U. H. F. Bunz, J. U. Engelhart, B. D. Lindner and M. Schaffroth, *Angew. Chem. Int. Ed.*, 2013, **52**, 3810–3821.
87 J. E. Anthony, J. S. Brooks, D. L. Eaton and S. R. Parkin, *J. Am. Chem. Soc.*, 2001, **123**, 9482–9483.
88 Y. Nicolas, F. Castet, M. Devynck, P. Tardy, L. Hirsch, C. Labrugère, H. Allouchi and T. Toupance, *Org. Electron.*, 2012, **13**, 1392–1400.
89 S. Jung, M. Albariqi, G. Gruntz, T. Al-Hathal, A. Peinado, E. Garcia-Caurel, Y. Nicolas, T. Toupance, Y. Bonnassieux and G. Horowitz, *ACS Appl. Mater. Interfaces*, 2016, **8**, 14701–14708.
90 J. Yao, Z. Cai, Z. Liu, C. Yu, H. Luo, Y. Yang, S. Yang, G. Zhang and D. Zhang, *Macromolecules*, 2015, **48**, 2039–2047.
91 H. Xin and X. Gao, *ChemPlusChem*, , DOI:10.1002/cplu.201700039.
92 J.-X. Dong and H.-L. Zhang, *Chin. Chem. Lett.*, 2016, **27**, 1097–1104.
93 T. M. Pappenfus, R. J. Chesterfield, C. D. Frisbie, K. R. Mann, J. Casado, J. D. Raff and L. L. Miller, *J. Am. Chem. Soc.*, 2002, **124**, 4184–4185.
94 R. J. Chesterfield, C. R. Newman, T. M. Pappenfus, P. C. Ewbank, M. H. Haukaas, K. R. Mann, L. L. Miller and C. D. Frisbie, *Adv. Mater.*, 2003, **15**, 1278–1282.
95 S. Handa, E. Miyazaki, K. Takimiya and Y. Kunugi, *J. Am. Chem. Soc.*, 2007, **129**, 11684–11685.
96 D. E. Janzen, M. W. Burand, P. C. Ewbank, T. M. Pappenfus, H. Higuchi, D. A. da Silva Filho, V. G. Young, J.-L. Brédas and K. R. Mann, *J. Am. Chem. Soc.*, 2004, **126**, 15295–15308.
97 Z. Yan, B. Sun and Y. Li, *Chem. Commun.*, 2013, **49**, 3790.
98 T. Lei, J.-H. Dou, X.-Y. Cao, J.-Y. Wang and J. Pei, *J. Am. Chem. Soc.*, 2013, **135**, 12168–12171.
99 G. Zhang, P. Li, L. Tang, J. Ma, X. Wang, H. Lu, B. Kang, K. Cho and L. Qiu, *Chem. Commun.*, 2014, **50**, 3180–3183.
100 A. Baeyer, *Berichte Dtsch. Chem. Ges.*, 1879, **12**, 1309–1319.
101 M. Sommer, *J. Mater. Chem. C*, 2014, **2**, 3088–3098.
102 X. Guo and M. D. Watson, *Org. Lett.*, 2008, **10**, 5333–5336.
103 Z. Chen, Y. Zheng, H. Yan and A. Facchetti, *J. Am. Chem. Soc.*, 2009, **131**, 8–9.
104 X. Guo, F. S. Kim, M. J. Seger, S. A. Jenekhe and M. D. Watson, *Chem. Mater.*, 2012, **24**, 1434–1442.
105 F. S. Kim, X. Guo, M. D. Watson and S. A. Jenekhe, *Adv. Mater.*, 2010, **22**, 478–482.
106 T. Schuettfort, L. Thomsen and C. R. McNeill, *J. Am. Chem. Soc.*, 2013, **135**, 1092–1101.
107 N. Zhou, H. Lin, S. J. Lou, X. Yu, P. Guo, E. F. Manley, S. Loser, P. Hartnett, H. Huang, M. R. Wasielewski, L. X. Chen, R. P. H. Chang, A. Facchetti and T. J. Marks, *Adv. Energy Mater.*, 2014, **4**, 1300785.
108 K. D. Deshmukh, T. Qin, J. K. Gallaher, A. C. Y. Liu, E. Gann, K. O'Donnell, L. Thomsen, J. M. Hodgkiss, S. E. Watkins and C. R. McNeill, *Energy Environ. Sci.*, 2014, **8**, 332–342.
109 C. Mu, P. Liu, W. Ma, K. Jiang, J. Zhao, K. Zhang, Z. Chen, Z. Wei, Y. Yi, J. Wang, S. Yang, F. Huang, A. Facchetti, H. Ade and H. Yan, *Adv. Mater.*, 2014, **26**, 7224–7230.
110 H. Kang, M. A. Uddin, C. Lee, K.-H. Kim, T. L. Nguyen, W. Lee, Y. Li, C. Wang, H. Y. Woo and B. J. Kim, *J. Am. Chem. Soc.*, 2015, **137**, 2359–2365.
111 W. Lee, C. Lee, H. Yu, D.-J. Kim, C. Wang, H. Y. Woo, J. H. Oh and B. J. Kim, *Adv. Funct. Mater.*, 2016, **26**, 1543–1553.
112 Y. Kim, D. X. Long, J. Lee, G. Kim, T. J. Shin, K.-W. Nam, Y.-Y. Noh and C. Yang, *Macromolecules*, 2015, **48**, 5179–5187.
113 B. Kang, R. Kim, S. B. Lee, S.-K. Kwon, Y.-H. Kim and K. Cho, *J. Am. Chem. Soc.*, 2016, **138**, 3679–3686.
114 R. Kim, P. S. K. Amegadze, I. Kang, H.-J. Yun, Y.-Y. Noh, S.-K. Kwon and Y.-H. Kim, *Adv. Funct. Mater.*, 2013, **23**, 5719–5727.
115 M. J. Sung, A. Luzio, W.-T. Park, R. Kim, E. Gann, F. Maddalena, G. Pace, Y. Xu, D. Natali, C. de Falco, L. Dang, C. R. McNeill, M. Caironi, Y.-Y. Noh and Y.-H. Kim, *Adv. Funct. Mater.*, 2016, **26**, 4984–4997.
116 Z. Zhao, Z. Yin, H. Chen, L. Zheng, C. Zhu, L. Zhang, S. Tan, H. Wang, Y. Guo, Q. Tang and Y. Liu, *Adv. Mater.*, 2017, **29**, 1602410.
117 Z. Zhao, Z. Yin, H. Chen, Y. Guo, Q. Tang and Y. Liu, *J Mater Chem C*, 2017, **5**, 2892–2898.
118 Z. Zhao, F. Zhang, Y. Hu, Z. Wang, B. Leng, X. Gao, C. Di and D. Zhu, *ACS Macro Lett.*, 2014, **3**, 1174–1177.
119 X. Zhan, Z. 'ao Tan, B. Domercq, Z. An, X. Zhang, S. Barlow, Y. Li, D. Zhu, B. Kippelen and S. R. Marder, *J. Am. Chem. Soc.*, 2007, **129**, 7246–7247.
120 X. Zhan, Z. 'ao Tan, E. Zhou, Y. Li, R. Misra, A. Grant, B. Domercq, X.-H. Zhang, Z. An, X. Zhang, S. Barlow, B. Kippelen and S. R. Marder, *J. Mater. Chem.*, 2009, **19**, 5794–5803.

121 W. Zhou, Y. Wen, L. Ma, Y. Liu and X. Zhan, *Macromolecules*, 2012, **45**, 4115–4121.
122 X. Zhao, L. Ma, L. Zhang, Y. Wen, J. Chen, Z. Shuai, Y. Liu and X. Zhan, *Macromolecules*, 2013, **46**, 2152–2158.
123 H. Li, F. S. Kim, G. Ren and S. A. Jenekhe, *J. Am. Chem. Soc.*, 2013, **135**, 14920–14923.
124 Y. Li, B. Sun, P. Sonar and S. P. Singh, *Org. Electron.*, 2012, **13**, 1606–1613.
125 C. Kanimozhi, N. Yaacobi-Gross, K. W. Chou, A. Amassian, T. D. Anthopoulos and S. Patil, *J. Am. Chem. Soc.*, 2012, **134**, 16532–16535.
126 P. Sonar, S. P. Singh, Y. Li, M. S. Soh and A. Dodabalapur, *Adv. Mater.*, 2010, **22**, 5409–5413.
127 W. Hong, B. Sun, H. Aziz, W.-T. Park, Y.-Y. Noh and Y. Li, *Chem. Commun.*, 2012, **48**, 8413.
128 B. Sun, W. Hong, E. Thibau, H. Aziz, Z.-H. Lu and Y. Li, *Org. Electron.*, 2014, **15**, 3787–3794.
129 B. Sun, W. Hong, E. S. Thibau, H. Aziz, Z.-H. Lu and Y. Li, *ACS Appl. Mater. Interfaces*, 2015, **7**, 18662–18671.
130 Y. Xiong, X. Qiao and H. Li, *Polym Chem*, 2015, **6**, 6579–6584.
131 B. Fu, C.-Y. Wang, B. D. Rose, Y. Jiang, M. Chang, P.-H. Chu, Z. Yuan, C. Fuentes-Hernandez, B. Kippelen, J.-L. Brédas, D. M. Collard and E. Reichmanis, *Chem. Mater.*, 2015, **27**, 2928–2937.
132 C. Guo, J. Quinn, B. Sun and Y. Li, *Polym. Chem.*, 2016, **7**, 4515–4524.
133 Z. Yuan, B. Fu, S. Thomas, S. Zhang, G. DeLuca, R. Chang, L. Lopez, C. Fares, G. Zhang, J.-L. Bredas and E. Reichmanis, *Chem. Mater.*, 2016, **28**, 6045–6049.
134 B. Sun, W. Hong, Z. Yan, H. Aziz and Y. Li, *Adv. Mater.*, 2014, **26**, 2636–2642.
135 B. Sun, W. Hong, H. Aziz and Y. Li, *Polym Chem*, 2015, **6**, 938–945.
136 J. Huang, Z. Mao, Z. Chen, D. Gao, C. Wei, W. Zhang and G. Yu, *Chem. Mater.*, 2016, **28**, 2209–2218.
137 W. Yue, M. Nikolka, M. Xiao, A. Sadhanala, C. B. Nielsen, A. J. P. White, H.-Y. Chen, A. Onwubiko, H. Sirringhaus and I. McCulloch, *J Mater Chem C*, 2016, **4**, 9704–9710.
138 T. Lei, J.-H. Dou, X.-Y. Cao, J.-Y. Wang and J. Pei, *Adv. Mater.*, 2013, **25**, 6589–6593.
139 Y. He, C. Guo, B. Sun, J. Quinn and Y. Li, *Polym. Chem.*, 2015, **6**, 6689–6697.
140 Y.-Z. Dai, N. Ai, Y. Lu, Y.-Q. Zheng, J.-H. Dou, K. Shi, T. Lei, J.-Y. Wang and J. Pei, *Chem. Sci.*, 2016, **7**, 5753–5757.
141 X. Zhou, N. Ai, Z.-H. Guo, F.-D. Zhuang, Y.-S. Jiang, J.-Y. Wang and J. Pei, *Chem. Mater.*, 2015, **27**, 1815–1820.
142 Y. Deng, B. Sun, Y. He, J. Quinn, C. Guo and Y. Li, *Angew. Chem. Int. Ed.*, 2016, **55**, 3459–3462.
143 Y. Deng, J. Quinn, B. Sun, Y. He, J. Ellard and Y. Li, *RSC Adv.*, 2016, **6**, 34849–34854.
144 J. Mei, D. H. Kim, A. L. Ayzner, M. F. Toney and Z. Bao, *J. Am. Chem. Soc.*, 2011, **133**, 20130–20133.
145 H. Chen, Y. Guo, G. Yu, Y. Zhao, J. Zhang, D. Gao, H. Liu and Y. Liu, *Adv. Mater.*, 2012, **24**, 4618–4622.
146 J. Yang, B. Xiao, K. Tajima, M. Nakano, K. Takimiya, A. Tang and E. Zhou, *Macromolecules*, 2017, **50**, 3179–3185.
147 Y. Li, P. Sonar, S. P. Singh, M. S. Soh, M. van Meurs and J. Tan, *J. Am. Chem. Soc.*, 2011, **133**, 2198–2204.
148 E. Wang, W. Mammo and M. R. Andersson, *Adv. Mater.*, 2014, **26**, 1801–1826.
149 W. Hong, S. Chen, B. Sun, M. A. Arnould, Y. Meng and Y. Li, *Chem Sci*, 2015, **6**, 3225–3235.
150 G. Zhang, J. Guo, M. Zhu, P. Li, H. Lu, K. Cho and L. Qiu, *Polym Chem*, 2015, **6**, 2531–2540.
151 S. M. Sze and K. K. Ng, *Physics of semiconductor devices*, Wiley-Interscience, Hoboken, N.J, 3rd ed., 2007.
152 H. Shirakawa, E. J. Louis, A. G. MacDiarmid, C. K. Chiang and A. J. Heeger, *J. Chem. Soc. Chem. Commun.*, 1977, 578–580.
153 H. Shirakawa, *Synth. Met.*, 2001, **125**, 3–10.
154 A. G. MacDiarmid, *Synth. Met.*, 2001, **125**, 11–22.
155 A. J. Heeger, *Synth. Met.*, 2001, **125**, 23–42.
156 K. Walzer, B. Maennig, M. Pfeiffer and K. Leo, *Chem. Rev.*, 2007, **107**, 1233–1271.
157 I. Salzmann and G. Heimel, *J. Electron Spectrosc. Relat. Phenom.*, 2015, **204**, 208–222.
158 S.-J. Yoo and J.-J. Kim, *Macromol. Rapid Commun.*, 2015, **36**, 984–1000.
159 B. Lüssem, M. Riede and K. Leo, *Phys. Status Solidi A*, 2013, **210**, 9–43.
160 J. Soeda, Y. Hirose, M. Yamagishi, A. Nakao, T. Uemura, K. Nakayama, M. Uno, Y. Nakazawa, K. Takimiya and J. Takeya, *Adv. Mater.*, 2011, **23**, 3309–3314.
161 T. Hähnel, C. Vanoni, C. Wäckerlin, T. A. Jung and S. Tsujino, *Appl. Phys. Lett.*, 2012, **101**, 033305.
162 F. Zhang, Y. Zang, D. Huang, C. Di, X. Gao, H. Sirringhaus and D. Zhu, *Adv. Funct. Mater.*, 2015, **25**, 3004–3012.
163 N. von Malm, J. Steiger, R. Schmechel and H. von Seggern, *J. Appl. Phys.*, 2001, **89**, 5559–5563.
164 R. Schmechel and H. von Seggern, *Phys. Status Solidi A*, 2004, **201**, 1215–1235.
165 H. T. Nicolai, M. Kuik, G. A. H. Wetzelaer, B. de Boer, C. Campbell, C. Risko, J. L. Br?das and P. W. M. Blom, *Nat. Mater.*, 2012, **11**, 882–887.
166 C. Li, L. Duan, H. Li and Y. Qiu, *J. Phys. Chem. C*, 2014, **118**, 10651–10660.
167 H. H. Fong, K. C. Lun and S. K. So, *Chem. Phys. Lett.*, 2002, **353**, 407–413.
168 C. Li, L. Duan, Y. Sun, H. Li and Y. Qiu, *J. Phys. Chem. C*, 2012, **116**, 19748–19754.
169 B. Lee, Y. Chen, D. Fu, H. T. Yi, K. Czelen, H. Najafov and V. Podzorov, *Nat. Mater.*, 2013, **12**, 1125–1129.
170 P. Wei, J. H. Oh, G. Dong and Z. Bao, *J. Am. Chem. Soc.*, 2010, **132**, 8852–8853.
171 B. D. Naab, S. Guo, S. Olthof, E. G. B. Evans, P. Wei, G. L. Millhauser, A. Kahn, S. Barlow, S. R. Marder and Z. Bao, *J. Am. Chem. Soc.*, 2013, **135**, 15018–15025.
172 B. D. Naab, S. Himmelberger, Y. Diao, K. Vandewal, P. Wei, B. Lussem, A. Salleo and Z. Bao, *Adv. Mater.*, 2013, **25**, 4663–4667.
173 W.-Y. Lee, H.-C. Wu, C. Lu, B. D. Naab, W.-C. Chen and Z. Bao, *Adv. Mater.*, 2017, **29**, 1605166.
174 S. Kazim, F. J. Ramos, P. Gao, M. K. Nazeeruddin, M. Gr?tzel and S. Ahmad, *Energy Env. Sci*, 2015, **8**, 1816–1823.
175 B. Sun, W. Hong, C. Guo, S. Sutty, H. Aziz and Y. Li, *Org. Electron.*, 2016, **37**, 190–196.
176 Y. He, J. T. E. Quinn, S. Lee, G. Y. Wang, X. Li, J. Wang and Y. Li, *Org. Electron.*, 2017, **49**, 406–414.
177 J. Quinn, H. Patel, F. Haider, D. A. Khan and Y. Li, *ChemElectroChem*, 2017, **4**, 256–260.
178 D. Khim, K.-J. Baeg, M. Caironi, C. Liu, Y. Xu, D.-Y. Kim and Y.-Y. Noh, *Adv. Funct. Mater.*, 2014, **24**, 6252–6261.
179 C. Liu, J. Jang, Y. Xu, H.-J. Kim, D. Khim, W.-T. Park, Y.-Y. Noh and J.-J. Kim, *Adv. Funct. Mater.*, 2015, **25**, 758–767.
180 J. Kim, D. Khim, K.-J. Baeg, W.-T. Park, S.-H. Lee, M. Kang, Y.-Y. Noh and D.-Y. Kim, *Adv. Funct. Mater.*, 2016, **26**, 7886–7894.
181 X. Zhao, D. Madan, Y. Cheng, J. Zhou, H. Li, S. M. Thon, A. E. Bragg, M. E. DeCoster, P. E. Hopkins and H. E. Katz, *Adv. Mater.*, 2017, 1606928.

View Article Online
DOI: 10.1039/C7TC01680H

182 T. Menke, D. Ray, H. Kleemann, K. Leo and M. Riede, *Phys. Status Solidi B*, 2015, **252**, 1877–1883.
183 M. L. Tietze, P. Pahner, K. Schmidt, K. Leo and B. Lüssem, *Adv. Funct. Mater.*, 2015, **25**, 2701–2707.
184 B. Lüssem, M. L. Tietze, H. Kleemann, C. Hoßbach, J. W. Bartha, A. Zakhidov and K. Leo, *Nat. Commun.*, 2013, **4**, 2775.
185 M. L. Tietze, F. Wölzl, T. Menke, A. Fischer, M. Riede, K. Leo and B. Lüssem, *Phys. Status Solidi A*, 2013, **210**, 2188–2198.
186 M. L. Tietze, B. D. Rose, M. Schwarze, A. Fischer, S. Runge, J. Blochwitz-Nimoth, B. Lüssem, K. Leo and J.-L. Brédas, *Adv. Funct. Mater.*, 2016, **26**, 3730–3737.
187 J.-M. Zhuo, L.-H. Zhao, R.-Q. Png, L.-Y. Wong, P.-J. Chia, J.-C. Tang, S. Sivaramakrishnan, M. Zhou, E. C.-W. Ou, S.-J. Chua, W.-S. Sim, L.-L. Chua and P. K.-H. Ho, *Adv. Mater.*, 2009, **21**, 4747–4752.
188 S. Guo, S. B. Kim, S. K. Mohapatra, Y. Qi, T. Sajoto, A. Kahn, S. R. Marder and S. Barlow, *Adv. Mater.*, 2012, **24**, 699–703.
189 Y. Qi, S. K. Mohapatra, S. Bok Kim, S. Barlow, S. R. Marder and A. Kahn, *Appl. Phys. Lett.*, 2012, **100**, 083305.
190 A. Higgins, S. K. Mohapatra, S. Barlow, S. R. Marder and A. Kahn, *Appl. Phys. Lett.*, 2015, **106**, 163301.
191 Y.-J. Hwang, H. Li, B. A. E. Courtright, S. Subramaniyan and S. A. Jenekhe, *Adv. Mater.*, 2016, **28**, 124–131.
192 Y. Lin and X. Zhan, *Mater. Horiz.*, 2014, **1**, 470–488.
193 A. Facchetti, *Mater. Today*, 2013, **16**, 123–132.
194 C. Lee, H. Kang, W. Lee, T. Kim, K.-H. Kim, H. Y. Woo, C. Wang and B. J. Kim, *Adv. Mater.*, 2015, **27**, 2466–2471.
195 B. T. McGrail, A. Sehirlioglu and E. Pentzer, *Angew. Chem. Int. Ed.*, 2015, **54**, 1710–1723.
196 Y. Chen, Y. Zhao and Z. Liang, *Energy Env. Sci*, 2015, **8**, 401–422.
197 M. Stolar and T. Baumgartner, *Phys. Chem. Chem. Phys.*, 2013, **15**, 9007–9024.
198 Y. Liang, Z. Chen, Y. Jing, Y. Rong, A. Facchetti and Y. Yao, *J. Am. Chem. Soc.*, 2015, **137**, 4956–4959.

View Article Online
DOI: 10.1039/C7TC01680H

Table of Content Entry

This article reviews recent major progress in the development of organic semiconductors as electron transport n-channel materials in organic field transistors (OFETs).